Journal of Building Engineering 46 (2022) 103664

Contents lists available at ScienceDirect

Journal of Building Engineering

journal homepage: www.elsevier.com/locate/jobe

Semi-active vibration control of building structure by Self Tuned Brain Emotional Learning Based Intelligent Controller

Muhammad Usman Saeed [a], Zuoyu Sun [a, *], Said Elias [b]

[a] School of Civil Engineering, Guangzhou University, Guangzhou, 510006, Guangdong, China
[b] Department of Construction Management and Engineering, University of Twente, Enschede, 7500 AE, Netherlands

ARTICLE INFO

Keywords:
Semi-active vibration control
Self-tuned brain emotional learning-based intelligent controller
Fuzzy logic
Fuzzy tuned PID

ABSTRACT

Control algorithms are the most crucial aspects in effective control of civil structures exposed to earthquake forces. Recently, adaptive intelligent control algorithms are evolving to be a viable substitute strategy for conventional model-based control algorithms. One of the most recent developments, known as the Brain Emotional Learning Based Intelligent Controller (BELBIC), has caught the attention of scientists as a model-free adaptive control system. It possesses appealing capabilities for dealing with nonlinearities and uncertainties in control frameworks. The modern semi-actively controlled civil structures have a highly uncertain and nonlinear nature following severe disturbances. As a result, these structures require real-time (online) robust control actions towards changing conditions, which the controllers with rigid settings cannot adapt. This study intends to overcome this issue in two ways: an online self-tuning brain emotional learning-based intelligent controller (ST-BELBIC) is formulated. Then its capabilities in improving the performance of cascaded controller in attenuating seismic vibrations of a three-story scaled building structure are validated. In this case, the central control unit BELBIC is based on sensory inputs (SI) and emotional cues (reward) signals. The main contribution of the proposed controller is a self-attuned version of the standard BELBIC that uses the benefits of a first-order Sugano fuzzy inference system (FIS) to adapt its parameters online. The proposed control methodology can be a promising model-free controller in terms of online tuning, simplicity of configuration, ease of applicability, less operational time, and neutralizing nonlinearities. The simulation affirms that the proposed controller compared with conventional LQR and intelligent Fuzzy tuned PID (FT-PID) controllers shows a superior performance regarding attenuating seismic responses of the building and can also improve the performance of cascaded FT-PID controller.

Nomenclature

ANNs	Artificial neural networks
AMY	Amygdale
APU	Amygdala Processing Unit

* Corresponding author.
E-mail addresses: muhammadusmansaeed@e.gzhu.edu.cn (M.U. Saeed), sunzuoyu@gzhu.edu.cn, sunzuoyu@gzhu.edu.cn (Z. Sun), elias.rahimi@utwente.nl (S. Elias).

https://doi.org/10.1016/j.jobe.2021.103664
Received 18 August 2021; Received in revised form 11 November 2021; Accepted 12 November 2021
Available online 27 November 2021

BEL	Brain emotional learning
BELBIC	Brain emotional learning-based intelligent controller
FT-PID	Fuzzy Tuned proportional integral derivative
FLC	Fuzzy logic control
PID	proportional integral derivative
FIS	Fuzzy inference system
LQR	Linear quadratic regulator
MFs	Membership functions
MRD	Magneto-rheological damper
MR	Magnetorheological
ORB	Orbitofrontal
OPU	Orbitofrontal Processing Unit
Rew	Reward
SI	Sensory Inputs
SC	Sensory Cortex
ST-BELBIC	Self-Tuned Brain emotional learning-based intelligent controller

1. Introduction

One of the most critical problems in structural engineering design is primary safety against destructive environmental forces such as earthquakes [1–4]. Many experts have contributed to passive and active vibration control systems incorporating theoretical and experimental approaches. The number of structures with active vibration control is undoubtedly less than those with passive vibration control [5–9].

When designing a structural system with active/semi-active control, the control framework may be planned such that the structure responds in a well-defined and explicit manner. The adequacy of active/semiactive control exceptionally relies upon the control algorithms requiring accurate and appropriate control gains for registering the actuator's control forces [10–12]. Overall, the critical establishment of the vibration control framework is control algorithms [13,39]. Moreover, these control algorithms help improve control schemes that are cost-effective, predictable, adaptive and robust, promoting progressively reliable, safe, lightweight, and vigorous structures [14,15].

In structural control, there are two types of active and semi-active control algorithms: (1) model-based control (MBC), which requires a mathematical model of the control system (linear, classic, and nonlinear controllers); and (2) Model-free. Model-free control is a method of controlling systems with complex dynamics and uncertainties without incurring system identification. In other terms, model-free control is defined as the capacity to construct a controller for a system based on a basic description of the system dynamics. Furthermore, various model-free intelligent control strategies have been recognized due to advances in soft computing techniques. These control algorithms are developed by replicating specific properties of intelligent biological systems in the subject of biologically inspired intelligent control. Many model-free control techniques, like artificial neural networks (ANNs) and fuzzy logic control (FLC), have been effective in a wide range of complex nonlinear civil structure control problems [16].

Corresponding Blachowski and Pnevmatiko [17] presented a study that used an ANNs controller to reduce seismic vibration, and their proposed controller was evaluated on two types of buildings: single-story and 12-story. When compared to the traditional LQR controller, the ANNs-based controller effectively lowered the structural response. Lara et al. [18] Presented two controllers; a feedback neural network named Nonlinear Auto-Regressive models with eXogenous Inputs (NARX-NNs) and FLC, to control a 2-story building structure equipped with MR damper. Their study evidenced that both these controllers had generated substantial results in reaching the control aim. The NARX-NNs-based controller, on the other hand, outperformed the FLC controller. Rathi et al. [19] presented a study based on an ANNs-based control algorithm for a seismically stimulated 2-story building coupled with an active tendon control system. The Lyapunov stability analysis ensures the stability of the error dynamics model. They concluded that the proposed controller had better stability and performance. Zabihi-Samani et al. [20] proposed an FLC control technique with three other algorithms: the discrete wavelet transform (DWT), the cuckoo search, and the geometrical nonlinearity algorithm. This proposed methodology was assigned the title as cuckoo-search wavelet-based fuzzy logic controller (AC-SWBFLC). They evaluated this new controller on a mathematical model of 3-story, 4-story, and 8-story buildings with MR-dampers undergoing seismic excitations. They found that this controller outperformed passive-off, passive-on, standard LQR, and FLC controllers. Bathaei et al. [21] Provided type-1 and type-2 Fuzzy Logic Control (FLC) for actuating a semi-active tuned mass damper with MR damper in an 11-DOF building model. Their findings revealed that both these controllers performed better specifically, the FLC type 2 controller outperformed the type 1 controller. Finally, in Faraji [22] study, an FLC was reported for vibration reduction of a single-story building equipped with MR damper, where the findings revealed that the FLC provided better performance.

The Brain Emotional Learning–Based Intelligent Controller (BELBIC), which simulates the emotional learning process in the limbic system in human brains, was recently introduced to this family of psycho biologically driven algorithms [23,24]. It's a sort of conditional learning linked to external emotional stimuli like rewards and punishments in real-life scenarios. The internal emotional states such as joy, sadness, and fear might be triggered by these emotional cues, influencing future decisions. The brain emotional learning (BEL) algorithm concept was first proposed in Refs. [25,26] by MorÉn et al. Since then, the BELBIC has become more widely

employed in various control engineering applications, including electric motors, servo systems, motion control, control effort reduction, and power systems, among others [27].

The BELBIC is a model-free controller with a simplistic control framework. The online learning capacity, minimal computational complexity, and, most importantly, no need for prior knowledge of system dynamics makes BELBIC a distinctive controller over formerly debated intelligent controllers, such as ANNs and FLC. Furthermore, it is simple, with fewer tuning parameters in emotional controllers, and, unlike traditional ANNS, it doesn't require an additional iterative process for learning or updating parameters [28]. Contrasting, in neural network control, the network topology, like that of the number of layers, nodes, and parameters in the activation functions, are critical considerations that must be considered appropriately [29]. In addition, there are various tuning factors in FLC, such as the center and width of the Gaussian membership functions and the weight of each rule. The adaptation laws are obtained from stability analysis to alter these values. Furthermore, the starting values of these parameters and their convergence rate seem to significantly impact the controller's effectiveness and, therefore, should be carefully determined. After doing all that, this still does not adequately handle unknown system dynamics [30,31]. In contrast to all of these concerns, the BELBIC has produced very satisfactory outcomes. The BELBIC is an efficient controller in addressing highly complicated and nonlinear problems based on its two principal inputs: Sensory Input (SI) and Primary Reward (Rew), and the flexibility in defining SI and Rew. Additionally, BELBIC also can learn for displaying responses similar to robust adaptive approaches.

Assigning a suitable parameter for Rew and SI is crucial for using BELBIC to regulate a system correctly. Until recently, there hasn't been a specified mathematical strategy for tuning the BELBIC [32]. There are a few methods for tuning the parameters of BELBIC. These methods include the trial-and-error method [33], or are based on the result of a cost function optimization using evolutionary-based algorithms (particle swarm optimization (PSO) algorithm [34–38] and clonal selection algorithm) [40] and Lyapunov based algorithm [41]. Even some recent research utilises intelligent techniques such as fuzzy logic to tune its parameters [42,43].

The use of BELBIC for the control of smart civil structures has gotten a lot of attention in recent years. In which BELBIC was utilized to reduce the vibration response of a Single Degree of Freedom (SDOF) building structure equipped with a Magneto-Rheological (MR) damper in a numerical study proposed by César et al., [33]. In this study, the author used the most popular trial and error method to adjust the fixed parameters of BELBIC's Rew and SI signals. In contrast, in some situations, the adaptive controller's performance from these fixed-tuned parameters was insufficient. Its parameters had to be chosen only by designers based on the control problem, and it is challenging to determine these control parameters precisely. Furthermore, in smart civil structure vibration control, a few studies have reported an offline parameter optimization strategy for the BELBIC controller. The parameters were developed using an evolutionary search technique such as particle swarm optimization (PSO) algorithm. As César et al. [36], presented a study of seismic vibration control of SDOF building structure equipped with MR damper where the authors have utilized the capabilities of PSO for the tuning of BELBIC, Rew and SI parameters. One more study was reported by Braz César et al. [35], in which a three-story seismically excited building equipped with MR damper have been controlled by PSO optimized BELBIC. Both of these investigations used offline tuning techniques, as previously mentioned. The offline tuning of controllers necessitates a lengthy training period and a significant amount of computing time. Furthermore, it cannot adapt to real-time control systems, and mistuning can directly impact control performance [44,45].

Since a semi-active control of the civil structural system is highly nonlinear, complex, and uncertain due to lack of knowledge of some parameters or external disturbances. Thus, a controller design that can react quickly to these challenges in real-time/online is required. The usage of fuzzy inference systems (FIS) is a suitable approach for updating the parameters of the BELBIC controller online. Moreover, the FIS typically replicates human knowledge and reasoning processes without requiring precise mathematical models. The FIS enables data complexity to be reduced and uncertainty to be dealt with in real-time [46–48]. These benefits of FIS make it appealing for use as BELBIC's online-tuning process. The BEL's learning and FIS's reasoning capabilities collectively yield a substantially self-efficient controller against nonlinearities and uncertainties.

In this paper, an online Self Tuned-BELBIC (ST-BELBIC) controller will be applied for the semiactive case of attenuating the building structure's seismic response. The BELBIC is developed for the structural system as its primary controller, and the FIS is developed regarding the system characteristics and expert knowledge to online tune the BELBIC's parameters. The proposed controller includes a PID cascaded controller structure. Thus the application of FIS towards PID could be characterized here as a combination of fuzzy logic principles with the standard PID controller [49]. Consequently, using FIS essentially allows the BELBIC to self-tune its parameters in real-time operation, compensating for the BELBIC's internal instability and challenges.

The present paper is organized as follows: The semi-active structural system defining building structure and Magneto-Rheological Damper (MRD) is presented in Section 2. The proposed ST-BELBIC system design is discussed in Section 3, some results and discussions follow the paper in Section 4, and the paper is concluded with several brief notes in Section 5.

2. Semi-active structural system

2.1. Modelling of the building structure

The performance of the developed system of control is tested in this study using a three-story scaled building structure taken from the existing literature [50], as shown in Fig. 1. The building is trialed using a semi-active control method and has an MR-damper mounted on each story. The mass, stiffness, and damping matrices developed for the building structure are given in eqs. (1)–(3).

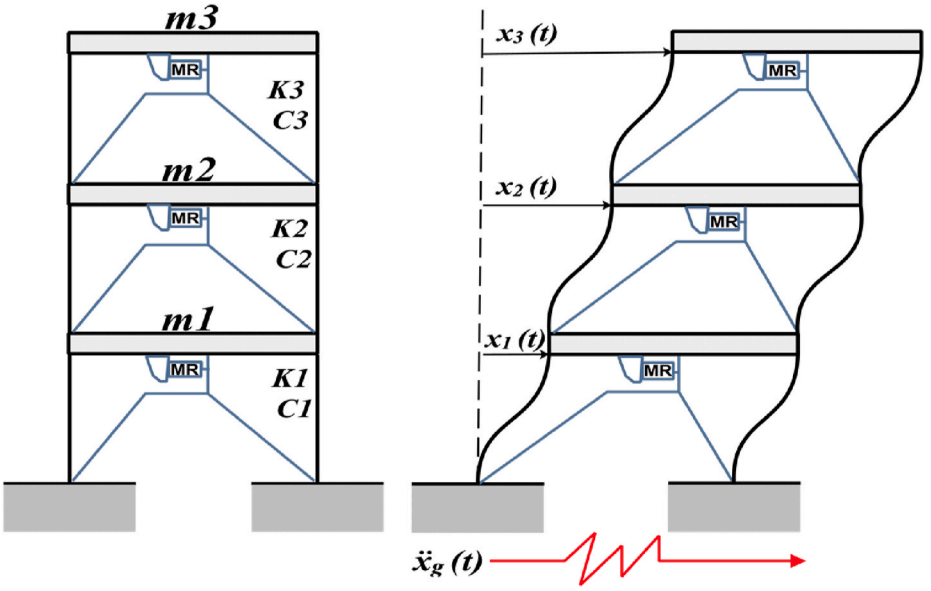

Fig. 1. 3-story building system equipped with MR damper under earthquake loading.

$$\mathbf{M} = \begin{bmatrix} 98.3 & 0 & 0 \\ 0 & 98.3 & 0 \\ 0 & 0 & 98.3 \end{bmatrix} \text{kg} \tag{1}$$

$$\mathbf{K} = \begin{bmatrix} 12 & -6.84 & 0 \\ -6.84 & 13.7 & -6.84 \\ 0 & -6.84 & 6.84 \end{bmatrix} \times 10^5 \frac{\text{N}}{\text{m}} \tag{2}$$

$$\mathbf{C}_d = \begin{bmatrix} 175 & -50 & 0 \\ -50 & 100 & -50 \\ 0 & -50 & 50 \end{bmatrix} \frac{\text{N.s}}{\text{m}} \tag{3}$$

2.1.1. State equations

The equation of motion of a 3-story building structure with the MR-damper can be written in the matrix form as

$$\mathbf{M}\,\ddot{\boldsymbol{x}}(t) + \mathbf{C}_d\dot{\boldsymbol{x}}(t) + \mathbf{K}\;\boldsymbol{x}(t) = \boldsymbol{\Gamma}\boldsymbol{f}_c(t) + \mathbf{M}\boldsymbol{\lambda}\ddot{x}_g(t) \tag{4}$$

$$\lambda = \{-1\ -1\ -1\}^T,\ \boldsymbol{\Gamma} = \begin{bmatrix} -1 & 1 & 0 \\ 0 & -1 & 1 \\ 0 & 0 & -1 \end{bmatrix},\ \boldsymbol{f}_c(t) = \begin{Bmatrix} f_{c1}(t) \\ f_{c2}(t) \\ f_{c3}(t) \end{Bmatrix} \text{ and } \boldsymbol{x}(t) = \begin{Bmatrix} x_1(t) \\ x_2(t) \\ x_3(t) \end{Bmatrix} \tag{5}$$

M, $\mathbf{C}_d$, **K** are mass, damping, and stiffness matrices as defined in equations (1)–(3). $\boldsymbol{x}$(t) defines the displacement response, and $\boldsymbol{\lambda}$ represent the disturbance force vector. As in this example, the semi-active MRD are installed on each story of structure the coefficient of MR damping force matrix is represented by $\boldsymbol{\Gamma}$ where, each column represents the damper force coefficients of first, second and third story as given by $\boldsymbol{\Gamma}_{\boldsymbol{1st}}^T = [-1\ 0\ 0];\boldsymbol{\Gamma}_{\boldsymbol{2nd}}^T = [1\ -1\ 0]$ *and*; $\boldsymbol{\Gamma}_{\boldsymbol{3rd}}^T = [0\ 1\ -1]$. These coefficient matrices and vectors are defined as given in eq. (5). $\boldsymbol{f}_c(t)$ as given in equation (5) is the vector of controlled damping force provided by MR damper, which is calculated by proposed self-tuned Brain Emotional learning-based intelligent Controller (ST-BELBIC) and $\ddot{x}_g(t)$ represents the disturbance (ground excitation) force. By defining the state vector as $\boldsymbol{z}(t) = \begin{Bmatrix} \boldsymbol{x}(t) \\ \dot{\boldsymbol{x}}(t) \end{Bmatrix}$, the governing equation (4) can be rewritten in the state-space form as given by

$$\dot{\boldsymbol{z}}(t) = \mathbf{A}\;\boldsymbol{z}(t) + \mathbf{B}\;\boldsymbol{f}_c(t) - \boldsymbol{E}\ddot{x}_g(t)$$

$$where, \mathbf{A} = \begin{bmatrix} \mathbf{0} & \mathbf{I} \\ -\mathbf{M}^{-1}\mathbf{K} & -\mathbf{M}^{-1}\mathbf{C}_d \end{bmatrix}; \mathbf{B} = \begin{bmatrix} \mathbf{0} \\ \mathbf{M}^{-1}\boldsymbol{\Gamma} \end{bmatrix}; \boldsymbol{E} = \begin{Bmatrix} \mathbf{0} \\ \boldsymbol{\lambda} \end{Bmatrix}; \tag{6}$$

$$\boldsymbol{y}(t) = \mathbf{C}\ \boldsymbol{z}(t) + \mathbf{D}_c\ \boldsymbol{f}_c(t) - \boldsymbol{D}_g \ddot{x}_g(t)$$

$$where,\ \mathbf{C} = \begin{bmatrix} \mathbf{I} & \mathbf{0} \\ \mathbf{0} & \mathbf{I} \\ -\mathbf{M}^{-1}\mathbf{K} & -\mathbf{M}^{-1}\mathbf{C}_d \end{bmatrix};\ \mathbf{D}_c = \begin{bmatrix} \mathbf{0} \\ \mathbf{M}^{-1}\boldsymbol{\Gamma} \end{bmatrix}\ and\ \boldsymbol{D}_g = \begin{Bmatrix} \mathbf{0} \\ \lambda \end{Bmatrix} \tag{7}$$

In eq. (6), the state vector size is (2n × 1); $\mathbf{A} \in \mathbb{R}^{2n\times 2n}$ represents the system matrix; $\mathbf{B} \in \mathbb{R}^{2n\times n}$ matrix represents the location of input control force provided by the MR dampers and $\boldsymbol{E} \in \mathbb{R}^{2n\times 1}$ represents the input location of the disturbance force. In eq. (7) the $\boldsymbol{y}$ (t) $\in \mathbb{R}^{3n\times 1}$ is an output vector; $\mathbf{C} \in \mathbb{R}^{3n\times 2n}$ represents the output matrix and $\mathbf{D}_c \in \mathbb{R}^{3n\times n}$ *and* $\boldsymbol{D}_g \in \mathbb{R}^{3n\times 1}$ symbolizes the direct feedthrough matrix, respectively. In both these state equations $\mathbf{0} \in \mathbb{R}^{n\times n}$ and $\mathbf{I} \in \mathbb{R}^{n\times n}$ represent the null matrix and identity matrix, wherein $\mathbf{D}_c, \mathbf{0} \in \mathbb{R}^{2n\times n}$, $\boldsymbol{D}_g, \mathbf{0} \in \mathbb{R}^{2n\times 1}$ and in $\boldsymbol{E}, \mathbf{0} \in \mathbb{R}^{2n\times 1}$ vector, where n represents the degrees of freedom (DOF).

2.2. Description of semi-active MR damper (MRD)-actuation system

The MRD became one of the most efficient semi-active structural vibration control devices due to its reported advantages of stability and reversibility. Whenever the structure is subjected to earthquake loads, aside from that, the MRD's high nonlinear dynamic behavior posed a significant obstacle for practical implementation in structural vibration control [51–53].

The MRD dampers are magneto-rheological fluid devices with a controllable fluid that could modify their rheological behavior as exposed to a magnetic field. The damper resistance force changes when the magneto-rheological fluid changes from liquid to semi-solid or solid in milliseconds. The Magneto-rheological Fluid has been the topic of various investigations and behavior modeling since its discovery. The plastic model of Bingham was the fundamental model of magneto-rheological fluid behavior. This Bingham model was created using the three constants Herschel–Bulkley fluid model, which considers the nonlinear flow of the rheological fluid [54].

Nonetheless, the Bingham model's simplicity has attracted the attention of various scholars, and it was developed into a standard linear model in Serial. On the other hand, these models were not created considering the hysteretic behaviour of the Magneto-rheological fluid. However, Bouc suggested a model explain this behaviour, which was later generalized by Wen and introduced the Bouc–Wen model. This model defines the relationship between displacement and force generated in a hysteretic way [55]. To completely practice the finest characteristics of the MR damper, Spencer et al. [56] proposed a modified version of the Bouc–Wen model, as shown in Fig. 2.

The central equation of the MRD force is determined by f_{MR} in equation (8), where $\dot{z}$ and z is the hysteretic displacement of the model, also called evolutionary variables given by the following equations:

$$f_{MR} = c_1\dot{y} + k_1(x - x_0) \tag{8}$$

$$\dot{z} = -\gamma\left|\dot{x} - \dot{y}\right|z|z|^{n-1} - \beta\ (\dot{x} - \dot{y})\,|z|^n + A(\dot{x} - \dot{y}) \tag{9}$$

$$and\ \dot{y} = \frac{1}{c_0 + c_1}\{\alpha z + c_0\ \dot{x} + k_0\ (x - y)\} \tag{10}$$

And the dependent variables on the applied voltage (u) to the current driver and the resulting magnetic current are presented as follows [56].

$$\alpha = \alpha(u) = \alpha_a + \alpha_b u \tag{11}$$

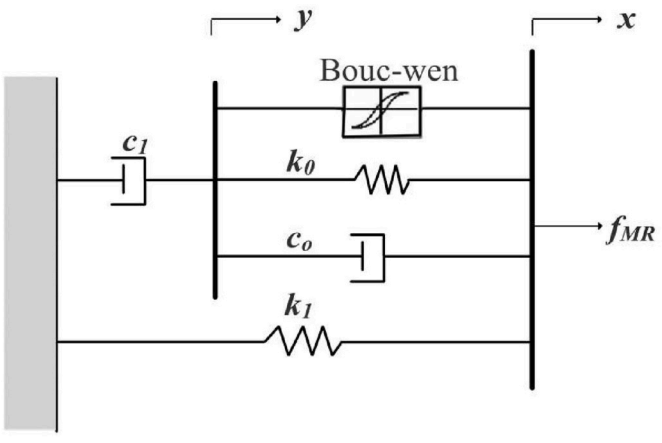

Fig. 2. Simple mechanical model of MRD.

$$c_1 = c_1(u) = c_{1a} + c_{1b}u \tag{12}$$

$$c_0 = c_0(u) = c_{0a} + c_{0b}u \tag{13}$$

Where u is a first-order filtered version of supplied voltage v is given by

$$\dot{u} = -\eta\,(u - v) \tag{14}$$

where x and $\dot{x}$ represent the device's displacement and velocity, f_{MR} and z are the device's generated force and hysteretic component, k_0 and k_1 are the accumulator stiffness at low and high velocity, x_0 is the initial displacement of spring stiffness k_1, $c_{0,}$ and c_1 are the viscous damping at low and high velocity, γ, β, η, and A are parameters of the shape loop, u and v are the command input phenomenological variable and the command voltage applied to the device, η is a time constant of the first-order filter of the Bouc–Wen model and y is the displacement of the damping c_1. The parameters are presented in Table 1.

3. Control system design

In this section, the formulation of the proposed self-tuned BELBIC (ST-BELBIC) is explained.

3.1. Self-tuned brain emotional learning-based intelligent controller (BELBIC)

A fuzzy inference system was utilized in the anticipated controller model to formulate a data-driven adaptive intelligent controller for building structure vibration control. The BELBIC can be classified as a supervised network. The BELBIC is simple to use and has a fast convergence rate; it can be used in various nonlinear control systems. The essential features of the proposed method involve fast training, methods for rules inserting and adjusting controller's parameters online. The basic mathematical structure of BELBIC is defined in the following section.

3.1.1. Structure

The BELBIC is a learning controller centered upon Moran's limbic structure's computational model known as brain emotional Learning (BEL) [16]. This structure is a simplified representation of the limbic system's principal components. These components include the amygdale (AMY), orbitofrontal cortex (ORB), thalamus, and sensory cortex (CS). The BELBIC model's structure and connections between parts can be best depicted through a Simulink block presented by Coelho, Pinho [57] as depicted in Fig. 3. The thalamus is the first place where sensory input (SI) information is processed. The sensory cortex (SC) and amygdale (AMY) units receive input signals after this step of pre-processing. The SC is in charge of separating the coarse output from the thalamus. Later, the filtered signal is then transmitted to the amygdale (AMY) and orbitofrontal (ORB) cortexes. The AMY is a tiny region inside the brain's medial temporal lobe responsible for the emotional evaluation of stimuli [16]. One of the more central part of the limbic system is the orbitofrontal cortex (ORB). The ORB responsible for inhibiting improper amygdale responses. The mathematical structure of each processing unit of BELBIC can be defined concerning each DOF is explained as follows [48,57].

1. Thalamus: has a data transfer function that sends SI to SC and maximum (SI) to AMY, according to Eq. (15) (see Fig. 3).

$$SI_{th} = \max(SI_i) \tag{15}$$

In eq. (15), the input signals from the SC to AMY include SI, while the one coming from the thalamus is SI_{th} which is the SI's maximum to simulate the uncertain data received from the thalamus. Furthermore, ORB's input patterns received from the sensory cortex are SI.

2. *Sensory Cortex:* Fig. 3 shows that the output of the thalamus is received into the ORB and AMY cortexes. It signifies that the signal is not obstructed in any way. In formula (16-18), the output of the AMY and ORB cortexes can be computed for ith sensory input (SI_i).

$$A_i = SI_i V_{A,i} \tag{16}$$

Table 1
Parameter of SD-1000 MRD model [56].

Parameter	Value	Parameter	Value
c_{0a}	21.0 N s cm^{-1}	c_{1a}	283 N s cm^{-1}
c_{0b}	3.5 N s cm^{-1} V^{-1}	c_{1b}	2.95 N s cm^{-1} V^{-1}
k_0	46.9 N cm^{-1}	k_1	5.00 N cm^{-1}
x_0	14.3 cm	γ	363 cm^{-2}
n	2	η	190 s^{-1}
α_a	140 N cm^{-1}	α_b	695 N cm^{-1} V^{-1}
A	301	β	363 cm^{-2}

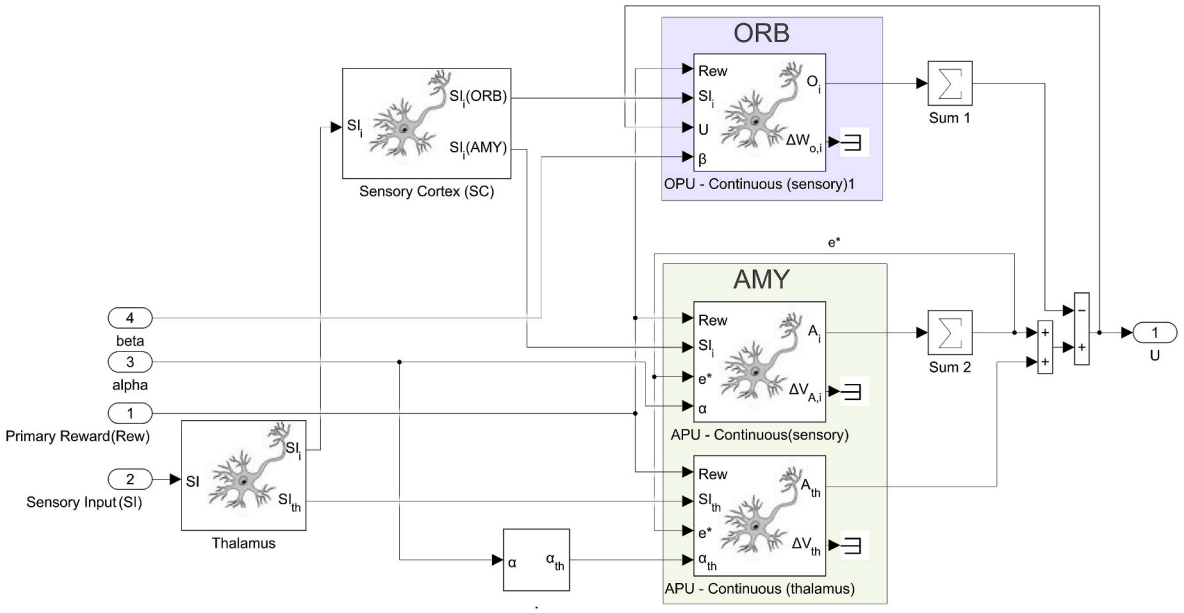

Fig. 3. Block diagram of the simplified limbic model (BEL) [57].

$$A_{th} = SI_{th} V_{th} \tag{17}$$

$$O_i = SI_i W_{o,i} \tag{18}$$

Where $V_{A,i}$, $V_{th,}$ and $W_{o,i}$ represent the associated weights of AMY and ORB cortexes, respectively.
The Model output U_i is computed using a formula (19), based on the output of the AMY and ORB cortexes.

$$U_i = \sum A_i - \sum O_i + A_{th} \tag{19}$$

3. *Amygdala and Orbitofrontal cortexes:* Learning in AMY and ORB cortexes can be calculated using formulas (20-22).

$$\Delta V_{th} = \alpha_{th} \left(\max \left[0, SI_i \left(\mathrm{Re}\, w - \left(\sum A_i \right) \right) \right] \right) \tag{20}$$

$$\Delta V_{A,i} = \alpha \left(\max \left[0, SI_i \left(\mathrm{Re}\, w - \left(\sum A_i \right) \right) \right] \right) \tag{21}$$

$$\Delta W_{o,i} = \beta \left(SI_i \left(e^* - \mathrm{Re}\, w \right) \right) \tag{22}$$

In the former formulas, α and β are learning rates utilized for regulating the rate of incorporating emotional inputs into the model output. As formula (20) and (21) show, the role of AMY is to guide output to create a link between *SI* and emotional cue (*Rew*) signals. In addition, as shown by formula (22), If the predicted signal does not match the reinforcement signal, output inhibition occurs in the ORB cortex.

4. *Development of sensory and emotional cues signals:* The BEL model has an open-loop structure, as evidenced by Fig. 3. The Modifications to meet control criteria are required before they may be utilized as the so-called BELBIC. The Rew function/Emotional signal and sensory inputs (*SI*) must incorporate specific feedback signals that create a closed-loop variant of the BELBIC. These signals were often described for structural control as either an arbitrary function of reference input, controller output, error between desired and measured response and plant/structure output (respose) [30,38]. Furthermore, the BELBIC gives flexibility to the designers to define these functions based on their needs (objectives). The overall performance of the BELBIC is greatly influenced by the definition of these signals [57].

- *Sensory Input*: In this study, *SI* is taken as the following function as presented in eq. (23).

$$SI_i = K_{pi}\, e_i(t) + K_{Ii} \int e_i(t)\, dt + K_{Di} \frac{d}{dt} e_i(t) + G_{1i}\, \ddot{x}_i(t) \tag{23}$$

- *Reward cue function:* The reward function will be formulated using the Proportional Integral Derivative (PID) control actions because of its parallel structure; it is suggested over the proportional integral (PI) and the proportional derivative (PD) control actions. When these actions were applied separately, they had limitations. The PD actions cannot affectively remove steady state

error; conversely, the PI action has poor performance in controlling the transient response of complex and nonlinear systems [49]. The Rew function is presented in eq. (24).

$$Rew_i = K_{pi}\, e_i(t) + K_{Ii} \int e_i(t)\, dt + K_{Di} \frac{d}{dt} e_i(t) + G_{2i} \int U_i\, dt \tag{24}$$

As given in eq. 20–24, $\boldsymbol{e}$ represents the error vector between desired displacement $\boldsymbol{x_r}$ (t) setpoint and the output value $\boldsymbol{x}$(t) of each DOF, $\ddot{x}(t)$ represents the acceleration response of the structure, and $\boldsymbol{U}$ represents the BELBIC's controller output, respectively. In common, $\boldsymbol{G_1}$, $\boldsymbol{G_2}$, $\boldsymbol{K_p}$,$\boldsymbol{K_I}$,$\boldsymbol{K_D}$, $\boldsymbol{\alpha}$ and $\boldsymbol{\beta} \in \mathbb{R}^{n\times 1}$ reflects model parameter's vectors corresponding to each DOF. Furthermore, sequentially, these parameters must be fine-tuned following input variables to attain the intended control action and increase control performance. Furthermore, when they are both fixed and mistuned, the system becomes unstable, making it increasingly challenging to provide the proper response under the influence of the system's nonlinearity and uncertainty [27,57,58]. Since the structure in this paper has nonlinear dynamic behaviour, fuzzy logic would be an appropriate tool, and online self tuned BELBIC can be developed for the structural vibration control as presented in Fig. 4.

3.1.2. Online tuning mechanism

As evidenced in Fig. 4 and given in eq. 21–24, the BELBIC parameters are divided into three separate groups: first, group deals with the coefficients of $\boldsymbol{Rew}$ signal as $\boldsymbol{K_P}$, $\boldsymbol{K_I}$, $\boldsymbol{K_D}$, and $\boldsymbol{G_2}$; a second, group of $\boldsymbol{SI}$ coefficients signal as $\boldsymbol{K_P}$, $\boldsymbol{K_I}$, $\boldsymbol{K_D}$, and $\boldsymbol{G_1}$ and third group deals with the learning rates in AMY and ORB cortexes: $\boldsymbol{\alpha}$ and $\boldsymbol{\beta}$. The First-order Sugano FIS is developed as an online tuning tool for the three groups of BELBIC's parameters in the proposed scheme; as a result, the proposed method for our nonlinear structural system can be developed directly. Thus, the nonlinearities present in both intelligent systems (BEL and FIS) can be dealt with using their in-built capabilities, i.e., the BEL has learning abilities and lacks reasoning abilities; conversely, the FIS has reasoning and lack learning abilities. Therefore, the online adaption of these parameters is made possible by introducing the seven adaptive parameters vectors as; $\boldsymbol{\Delta K_P}$, $\boldsymbol{\Delta K_I}$, $\boldsymbol{\Delta K_D}$, $\boldsymbol{\Delta G_1}$, $\boldsymbol{\Delta G_2}$, $\boldsymbol{\Delta\alpha}$, *and* $\boldsymbol{\Delta\beta}$. The basic working of this fuzzy logic tuner as depicted in Fig. 5, comprises four principal components: fuzzification, rule base, inference engine, and defuzzification. The fuzzifier linguistically converts/fuzzifies the controller input variables (measured from the structure/generated by the controller). The rule base comprises fuzzy rules that are if-then paraphrases, with antecedent and consequent statements in each rule. Furthermore, the inference engine generates each rule's output using fuzzy operations and mapping the input to the output. Finally, the defuzzification provides the crisp values of the adaptive parameters for our proposed control strategy [59].

Note that two ways of adjusting the MFs values/output values of a FIS can be adapted (1) For each FIS, their output range can be edited by doing adjustments (Scaling) in the MFs values. (2) secondly, it can be done by first adjusting the MFs to a fixed value and then adjusting the output values of FIS through introducing gain parameters for each adaptive parameter. In this study, we opted for

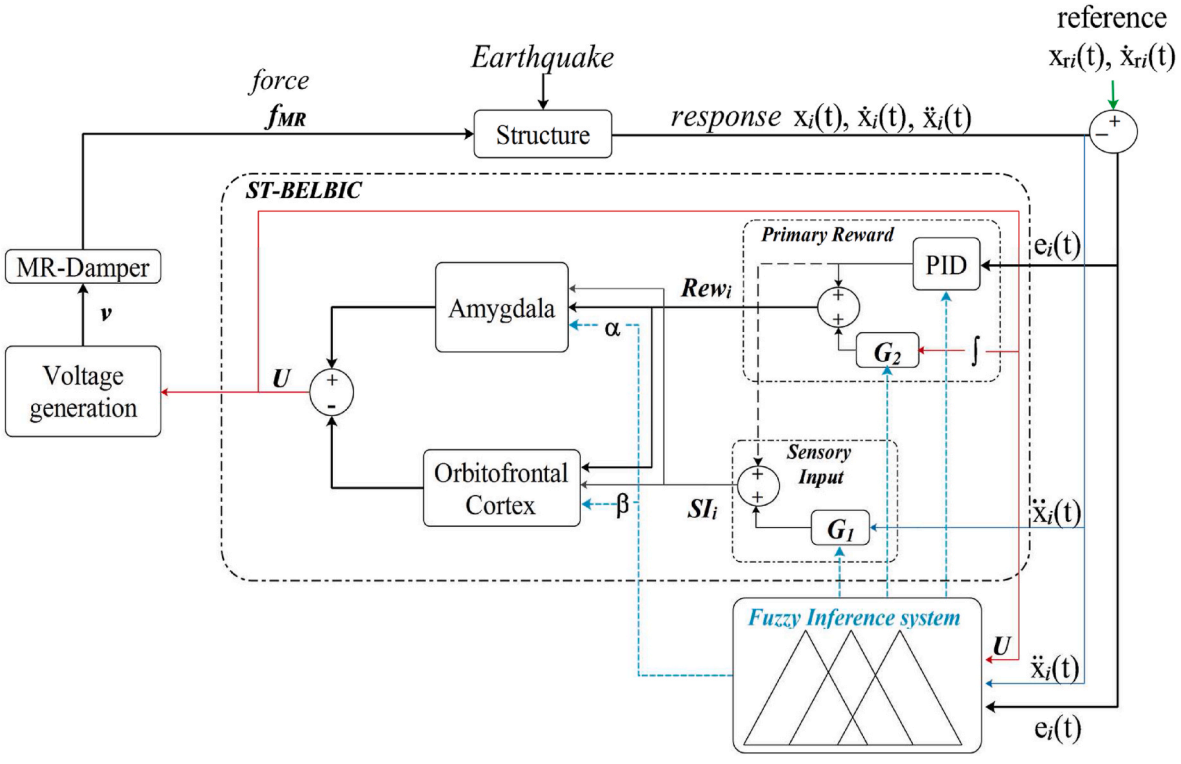

Fig. 4. Schematic of online Self-tuned brain emotional learning-based intelligent controller (ST-BELBIC).

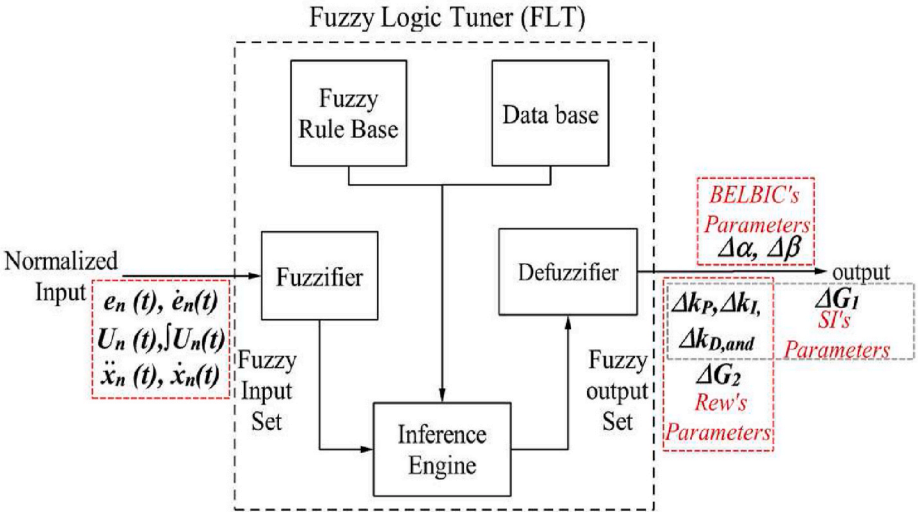

Fig. 5. Fuzzy logic tuner basic structure.

the second method; by doing so, the computational complexity of individually adjusting each MFs can be avoided, as seen in Fig. 6, where the g_P, g_I, g_D, g_1, g_2, g_α, and g_β presents the gains for adaptive parameters. Furthermore, the overall methodology of the proposed online self-tuned-Brain Emotional learning-based intelligent Controller (ST-BELBIC) is summarized in Fig. 6. In which each floor has its BELBIC. Furthermore, each response signal has its own FIS for computing corresponding adaptive parameters. The proposed control algorithm is implemented by using BELBIC, fuzzy logic and Simulink tool boxes of matlab.

3.1.2.1. Self-tuned reward (Rew) function. The tuning mechanism for developing adaptive reward (***Rew***) function parameters is described in Fig. 6. The tuning consists of two separate entities that deal with tuning the PID controller parameters, and the other deals with the tuning of the $\boldsymbol{G_2}$ parameters. Their details are explained in the upcoming sub-sections.

1. *Fuzzy tuned PID:* The design algorithm of PID is developed to adjust the K_P, K_I, and K_D parameters online through FIS based on the error *e* (t) among the desired displacement set point and the output, as well as the derivation of error $\dot{e}$ (t) to ensure that the controlled structure has better dynamic and static performance. The general framework adapted is presented in Fig. 7, Where the PID parameters ($\boldsymbol{K_p}$, $\boldsymbol{K_I}$, $\boldsymbol{K_D}$) are defined based on the *i*th floor displacement's (x_i), error *e(t),* and its first derivative $\dot{e}$ *(t),* as presented in the following equations.

$$e_i(t) = x_i(t) - x_{ri}(t) \tag{25}$$

$$\dot{e}_i(t) = \dot{x}_i(t) - \dot{x}_{ri}(t) \;\; or, \;\; e(t) - e(t-\tau) \tag{26}$$

here; $x_{ri}(t)$ and $\dot{x}_{ri}(t)$ represents the reference displacement and velocity response of the i-th floor (i = 1,2,3), respectively, and "τ" denotes the sampling time.

- *Fuzzification*: For the fuzzification of inputs e and $\dot{e}$ and to convert into suitable linguistic values, its ranges are defined as prescribed [e_{min}, e_{max}] and [$\dot{e}_{min}$, $\dot{e}_{max}$]. Their values need to be normalized for appropriateness in developing workable rule bases with greater inference efficiency as $e_n(t) \in [0,1]$ and $\dot{e}_n(t) \in [0,1]$. This normalization can be defined by following linear transformation functions.

$$e_n = \frac{e - e_{min}}{e_{max} - e_{min}} \tag{27}$$

$$\dot{e}_n = \frac{\dot{e} - \dot{e}_{min}}{\dot{e}_{max} - \dot{e}_{min}} \tag{28}$$

for each input variable (e_n and $\dot{e}_n$) 7 membership functions (MFs) are assigned as displayed in Fig. 8. These MFs names are "VS", "S", "MS", "M", "B", "MB" and, "VB" representing for "very small", "small", "medium small", "medium", "medium big", "big" and, "very big" respectively. Furthermore, For the fuzzification of output parameters $\boldsymbol{\Delta k_p}$, $\boldsymbol{\Delta k_I}$, and $\boldsymbol{\Delta k_D}$ represent the proportional, integral, and derivative modification variables. Furthermore, the values of these modification variables are assumed in fixed ranges as; $\Delta \boldsymbol{K_p} \in [0,150]$, $\Delta \boldsymbol{K_I} \in [0,20]$ and, $\Delta \boldsymbol{K_D} \in [0,200]$.

The linear output MFs names are taken the same as the input variables; These variables present the change in proportional and derivative gains that help the parameters of PID to adapt. Their relation is presented as below.

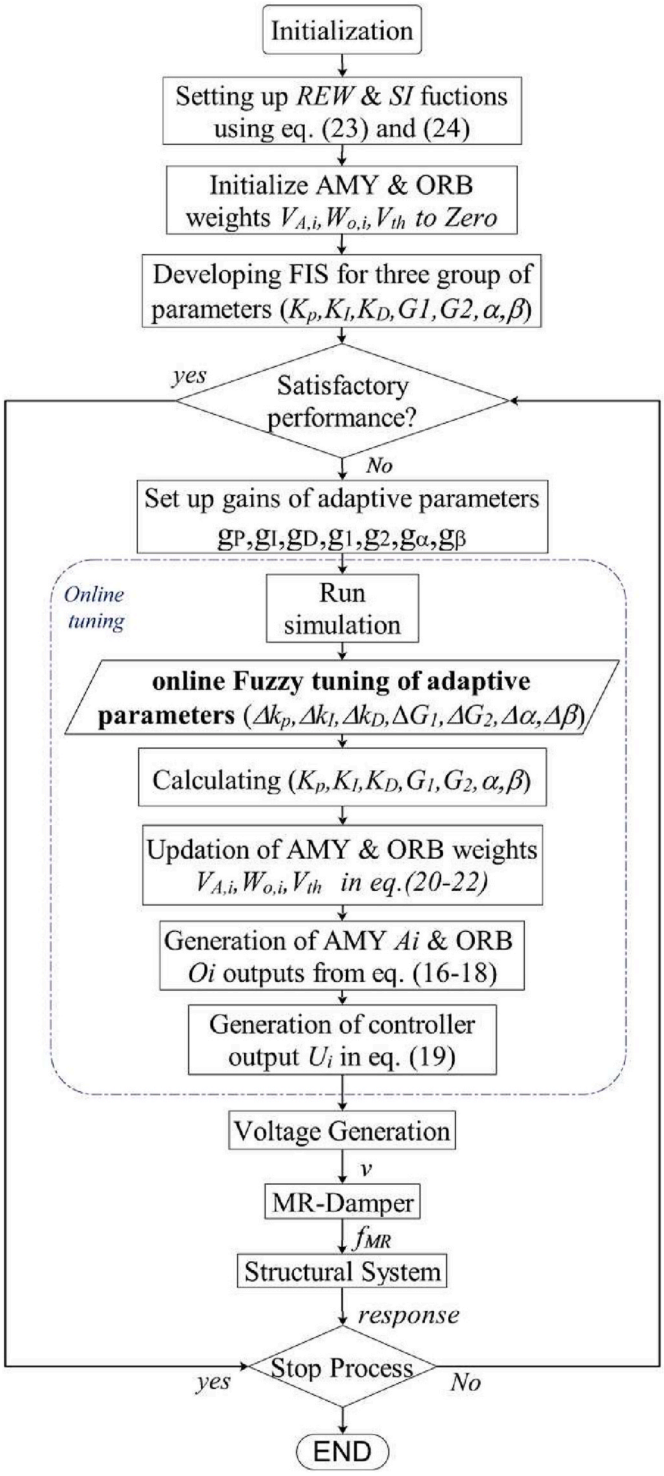

Fig. 6. Proposed design of Self-tuning BELBIC control of three-story building.

$$\boldsymbol{K}_p = \mathbf{g}_p \times \Delta \boldsymbol{k}_p \tag{29}$$

$$\boldsymbol{K}_I = \mathbf{g}_I \times \Delta \boldsymbol{k}_I \tag{30}$$

$$\boldsymbol{K}_D = \mathbf{g}_D \times \Delta \boldsymbol{k}_D \tag{31}$$

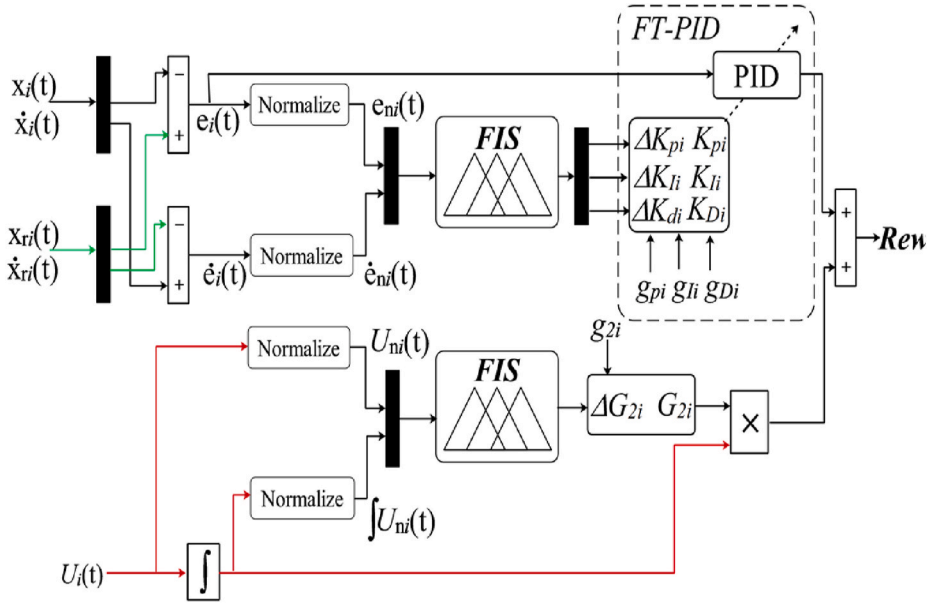

Fig. 7. Fuzzy online self-tuned reward parameters.

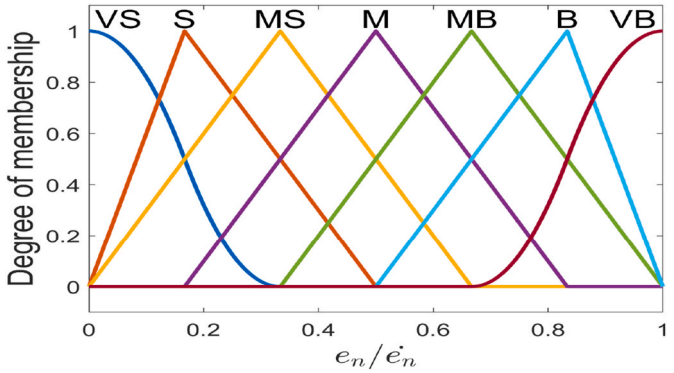

Fig. 8. MFs for inputs of FT-PID.

The g_P, g_I, and g_D are gain (multiplication) factors or modification coefficient constant values of proportional, integral, and derivative parameters.

- *Rule base and fuzzy inference:* A decision-making logic simulates a human decision process and aids in specifying a control strategy's input/output relation. The input e_n has seven linguistic labels and $\dot{e}_n$ also has seven linguistic labels. Therefore, we get a rule base consisting of $7 \times 7 = 49$ rules. These fuzzy rules are the outcome of numerous PID parameter tuning sessions. The rule base is simplified in Table 2.

Table 2
FIS rules table for fuzzy-PID online tuner.

$\Delta k_P/\Delta k_I/\Delta k_D$		$\dot{e}_n$ (t)						
		VS	S	MS	M	MB	B	VB
e_n(t)	VS	VB/VS/MB	VB/VS/MS	B/S/VS	B/S/VS	MB/MS/VS	M/M/S	M/M/MB
	S	VB/VS/MB	VB/VS/MS	B/S/VS	MB/MS/S	MB/MS/S	M/M/MS	MS/M/M
	MS	B/VS/M	B/S/MS	B/MS/S	MB/MS/S	M/M/MS	MS/MB/MS	MS/MB/M
	M	B/S/M	B/S/MS	MB/MS/MS	M/M/MS	MS/MB/MS	S/B/MS	S/B/M
	MB	MB/S/M	MB/MS/M	M/M/M	MS/MB/M	MS/MB/M	S/MB/M	S/VB/M
	B	MB/M/VB	M/M/MB	MS/MB/MB	S/MB/MB	S/B/MB	S/VB/MB	VS/VB/VB
	VB	M/M/VB	M/M/B	S/MB/B	S/B/B	S/B/MB	VS/VB/MB	VS/VB/VB

Furthermore, for simplicity, the result function is assumed to be a linear function to optimize the controller's computational efficiency, accuracy, and functionality, as presented in the following equation (32) for j^{th} rule.

$$\begin{aligned} &Rule\ j: if\ e_n(t)\ is\ H\ and\ \dot{e}_n(t)\ is\ P \\ &then\ f_i = p_{ij}e_n(t) + q_{ij}\dot{e}_n(t) + r_{ij} \end{aligned} \tag{32}$$

Where, j = 1, 2, …49 is the rule number, p_{ij},q_{ij}*and*r_{ij} are the i^{th} (constant) parameters of the result function. The *H* and *P* are fuzzy sets in the antecedent for e_n (t) and $\dot{e}_n$ (t) and, $f_i = f(e_n(t), \dot{e}_n(t))$ are the crisp functionally in the consequent or simply are the gains to be tuned, i.e., $\boldsymbol{\Delta k_p/\Delta k_I/\Delta k_D}$. Furthermore, the input and output relationship in a cartesian rule surface is presented in Fig. 9.

- *Defuzzification:* This outlines the process of converting a fuzzy inference into a crisp output. The weighted average approach is used to determine defuzzification. Thus, the exact value of $\boldsymbol{\Delta k_p}$, $\boldsymbol{\Delta k_I}$, $\boldsymbol{\Delta k_D}$ can be obtained, and then we can get the parameters of PID based on equations 29–31.

2. *Self-tuned* G_2*:* The formulation of the online tuned $\boldsymbol{G_2}$ parameter, a fuzzy tuned parameter $\boldsymbol{\Delta G_2}$, is introduced in the system having normalized inputs of the control signal $\boldsymbol{U}$; $\boldsymbol{U_n}$(t) and $\int \boldsymbol{U_n}$(t) as displayed in Fig. 7. Where the input MFs are presented in Fig. 10 as output MFs are taken as a linear result function having ranges as; $\Delta \boldsymbol{G_2} \in [0,1]$. The Fuzzy rules derived for this objective are presented in Table 3. The cartesian surface represented for the input/output mapping is presented in Fig. 11.

   As evidenced in Fig. 7, the value of the $\boldsymbol{G_2}$ parameter can be calculated as presented in eq. (33).

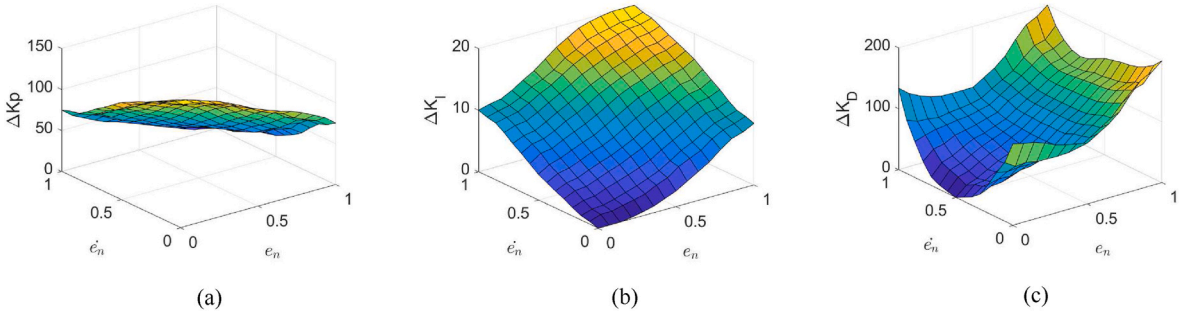

Fig. 9. Input and output relations in the form of Cartesian rule surface for $\boldsymbol{\Delta k_p}$, $\boldsymbol{\Delta k_I}$ and $\boldsymbol{\Delta k_D}$ parameters. (a) $\boldsymbol{\Delta k_p}$ surface; (b) $\boldsymbol{\Delta k_I}$ surface and; (c) $\boldsymbol{\Delta k_D}$ surface.

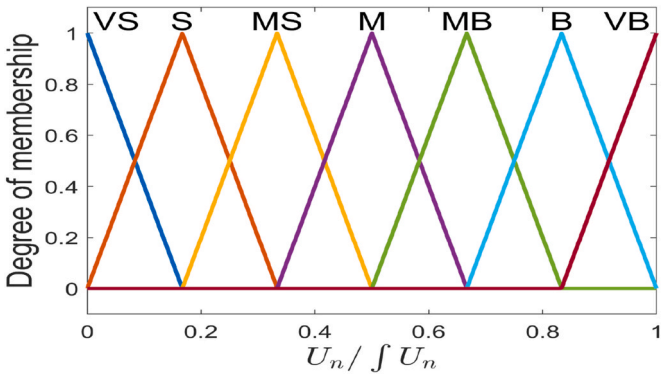

Fig. 10. MFs for inputs of $\Delta\ \boldsymbol{G_2}$.

Table 3
FIS rules table for fuzzy-tuned ΔG_2 parameter.

ΔG_2		$\int U_n$(t)						
		VS	S	MS	M	MB	B	VB
U_n(t)	VS	VS	S	MS	M	MS	MS	M
	S	S	S	MS	M	S	MS	MS
	MS	MS	MS	MS	M	S	S	S
	M	M	M	M	M	S	S	S
	MB	MS	S	S	S	S	S	S
	B	MS	MS	S	S	S	VS	VS
	VB	M	MS	S	S	S	VS	VS

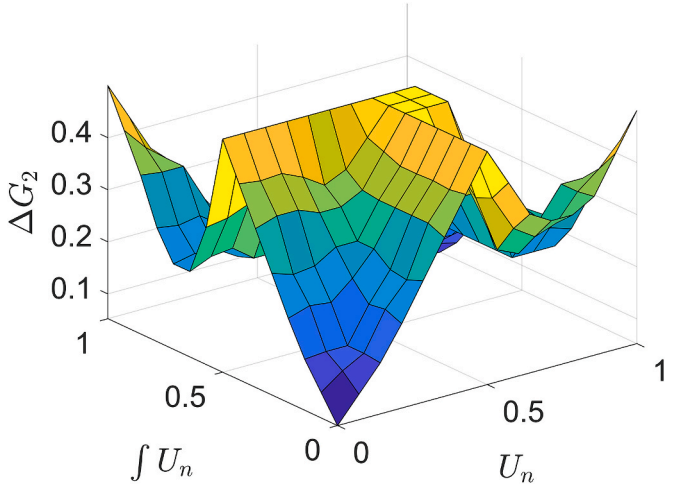

Fig. 11. Input and output relations in the form of Cartesian rule surface for ΔG_2.

$$G_2 = g_2 \times \Delta G_2 \tag{33}$$

The FIS generated values of ΔG_2 variable are multiplied with the g_2, which is a supervisor's or operator interacting constant vector gain and can be used to increase or decrease the rate/magnitude of the G_2 parameter to have control over the simulating system as a supervisor/explicit teacher. After the generation of G_2, it is then multiplied with the integral of the control signal (U) generated by the BELBIC controller that finally adds up with the fuzzy tuned PID to generate the overall Rew signal.

3.1.2.2. Self-tuned sensory input (SI) function. The parameters of SI as presented in Fig. 4 are calculated using adaptive parameters ΔG_1 and FT-PID's parameters as calculated in the previous section. For making ΔG_1 adaptable FIS is developed as presented in Fig. 12.

As presented in Fig. 12, the value of the G_1 parameter can be calculated as presented in eq. (34).

$$G_1 = g_1 \times \Delta G_1 \tag{34}$$

for the ΔG_1, the normalized input values of acceleration $\ddot{x}(t)$ response and integral of acceleration response $\dot{x}(t)$ of the structure is used as displayed in Fig. 12. The input MFs range for these normalized inputs is taken between [0,1] and shown in Fig. 13. The FIS rules among inputs and the outputs for ΔG_1 parameter are summarised in Table 4, and the cartesian surface is presented in Fig. 14. Additionally, the output MFs of SI function parameters ΔG_1 are range as $\Delta G_1 \in [0,10]$.

3.1.2.3. Self-tuned BELBIC's learning parameters (α and β). As presented in Fig. 3 and explained in eq. 20–22 the importance of learning rates of AMY/Amygdala Processing Unit (APU) and OFC/Orbitofrontal Processing Unit (OPU) can be noticed. As for the learning rate α is concerned it proper selection directs the weights $\Delta V_{A,i}$, ΔV_{th} towards a set of values that will eventually cause the minimization between *Rew* and partial amygdala signal $e^* = \sum A_i$ as an outcome. The AMY plays an essential role in seeking constant rewards. Furthermore, the learning rate β of OFC is similar to AMY. The main difference is that its selection helps increase or

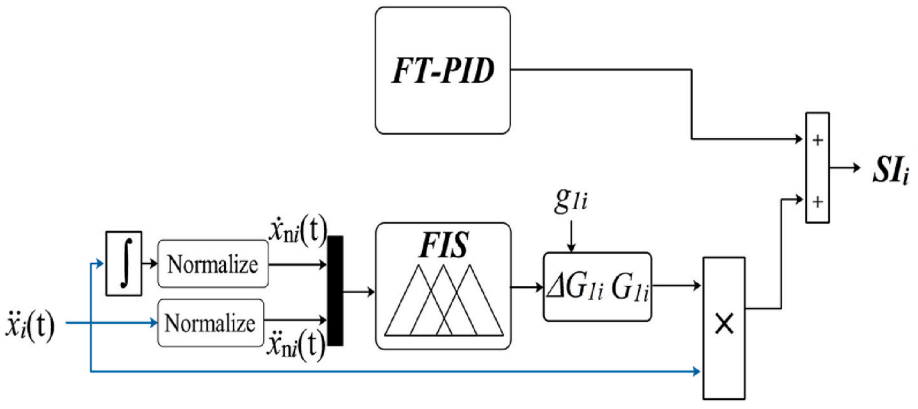

Fig. 12. FIS based online self-tuned Sensory Input parameters.

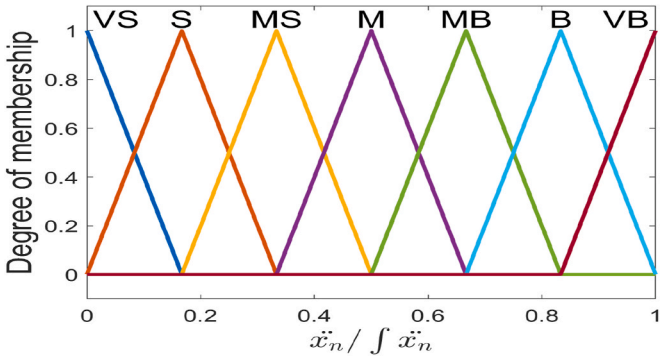

Fig. 13. MFs for inputs of ΔG_1.

Table 4
FIS rules table for fuzzy-tuned ΔG_1 parameter.

ΔG_1		$\int \ddot{x}_n$ (t)						
		VS	S	MS	M	MB	B	VB
$\ddot{x}_n$ (t)	VS	VS	VS	S	MS	M	MB	B
	S	VS	S	MS	M	MB	MB	B
	MS	S	MS	MS	M	MB	B	B
	M	MS	M	M	MB	MB	B	B
	MB	M	MB	MB	MB	MB	B	VB
	B	MB	MB	B	B	B	B	VB
	VB	B	B	B	B	VB	VB	VB

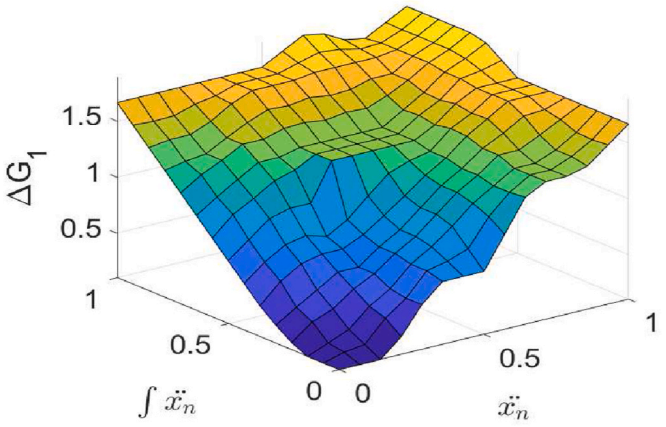

Fig. 14. Input and output relations in the form of Cartesian rule surface for ΔG_1.

decrease the tracking rate of weights of OFC as needed for proper inhibition. That unquestionably concludes that these learning rates significantly impact the actuation role of AMY and the preventer rule of OFC. Consequently, a rigorous selection procedure for tuning these parameters is needed to implement the BELBIC controller. Moreover, FIS is an appropriate tool for tuning these parameters in real-time to handle this situation. In this section, the development of FIS for tuning α and β is discussed. Similarly, their values are suggested to be in the range of α ∈[0,1] and β ∈[0,1] where 0 represents no learning and 1 represents instant adaptation [57].

The adaptive parameters of α and β are obtained by introducing two new parameters as Δα and Δβ, then the FIS for these parameters is developed based on normalized input values of e_n and $\dot{e}_n$. Whose input MFs are taken as triangular MFs, similar to as displayed in Fig. 13. Where as, the output MFs are taken as a linear result function having ranges $\Delta\boldsymbol{\alpha} \in[0,1]$ and $\Delta\boldsymbol{\beta} \in[0,0.04]$. Since, in the literature, the value of α is presumed to be greater than the one of β to track down the prior excitations contributions and thus inhibit output [57]. The rule base formulated for these adaptive learning parameters is presented in Table 5. The Cartesian rule surface representing the input and output relations for Δα and Δβ parameters is presented in Fig. 15 (a-b) After calculating FIS generated adaptive learning parameters, the final values of α and β parameters can be calculated as presented in the following equations.

Table 5
FIS rules table for **Δ**α and **Δ**β parameters.

Δ α / Δ β		$\dot{e}_n$ (t)						
		VS	S	MS	M	MB	B	VB
$e_n(t)$	VS	S	MS	MS	M	MB	MB	B
		VS	VS	VS	VS	VS	VS	S
	S	MS	MS	M	M	MB	B	B
		VS	VS	VS	VS	VS	VS	S
	MS	MS	M	M	M	MB	B	B
		VS	VS	VS	VS	VS	VS	MS
	M	M	M	MB	MB	MB	B	B
		VS	VS	VS	VS	S	MS	M
	MB	M	MB	MB	MB	B	B	B
		VS	VS	S	S	MS	M	MB
	B	MB	MB	MB	B	B	VB	VB
		S	S	S	MS	M	MB	B
	VB	MB	B	B	B	VB	VB	VB
		S	S	MB	M	MB	B	VB

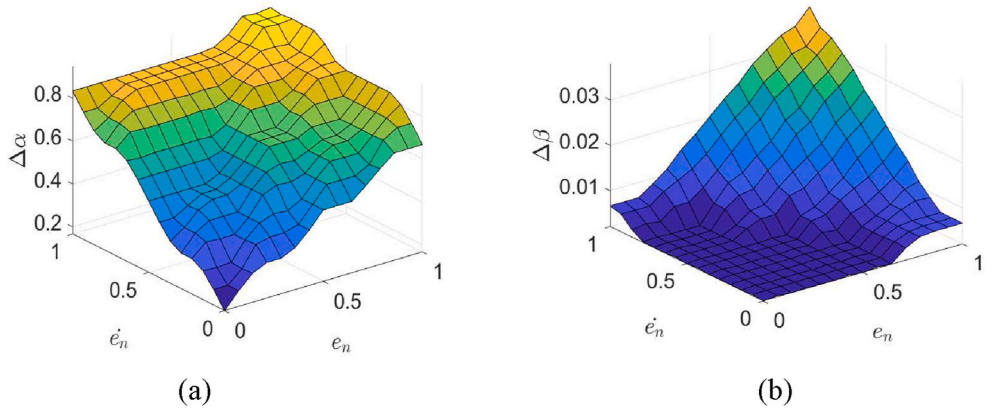

Fig. 15. Input and output relations in the form of Cartesian rule surface for Δα and Δβ parameters.

$$\alpha = g_{\alpha} \times \Delta_{\alpha} \tag{39}$$

$$\beta = g_{\beta} \times \Delta\beta \tag{40}$$

Where the principle of introducing two gain parameters ($\mathbf{g}_{\alpha}$*and*,$\mathbf{g}_{\beta}$) is the same as described in the earlier section.

3.1.2.4. Summary of design parameters of proposed ST-BELBIC. This section will summarise the design parameters used for the proposed control scheme. These parameters include the output MFs values as presented in Table 6 and the values of gain parameters presented in Table 7.

The FIS is a reasoning system that translates human reasoning into an inference system [60]. Therefore, the values of output MFs, gain parameters, and the developed inference rule base as given in the table (2–7) are based on experience (operators interactive iterative simulations) and expert knowledge (extensive literature review of different control studies under different operating condi-

Table 6
Summary of output MFs used in the proposed controller.

MFs	Adaptive Parameters						
	ΔKp	ΔK_I	ΔK_d	ΔG_1	ΔG_2	Δα	Δβ
MF1	[0 0 0]	[0 0 0]	[0 0 0]	[0 0 0.52]	[0 0 0.052]	[0 0 0.052]	[0 0 0.002]
MF2	[0 0 25.5]	[0 0 3.4]	[0 0 34]	[0 0 1.66]	[0 0 0.166]	[0 0 0.166]	[0 0 0.006]
MF3	[0 0 49.5]	[0 0 6.6]	[0 0 66]	[0 0 3.33]	[0 0 0.333]	[0 0 0.333]	[0 0 0.013]
MF4	[0 0 75]	[0 0 10]	[0 0 100]	[0 0 4.99]	[0 0 0.499]	[0 0 0.5]	[0 0 0.019]
MF5	[0 0 100.5]	[0 0 13.6]	[0 0 134]	[0 0 6.66]	[0 0 0.666]	[0 0 0.666]	[0 0 0.026]
MF6	[0 0 124.5]	[0 0 16.6]	[0 0 166]	[0 0 8.33]	[0 0 0.833]	[0 0 0.833]	[0 0 0.033]
MF7	[0 0 150]	[0 0 20]	[0 0 200]	[0 0 9.47]	[0 0 0.947]	[0 0 0.947]	[0 0 0.037]

Table 7
Gain parameters used in proposed.

Gains	Gain Vectors
	[DOF1 DOF2 DOF3]^T
$\mathbf{g}_p$	[-1.832e + 3 –1.725e + 3 –1.7836e + 3]^T
$\mathbf{g}_I$	[1.441e + 4 5e + 4 –2.8e + 4]^T
$\mathbf{g}_D$	[19 28 40]^T
$\mathbf{g}_1$	[2 1.84 0.64]^T
$\mathbf{g}_2$	[4.68 4.68 4.68]^T
$\mathbf{g}_\alpha$	[0.78 0.78 0.78]^T
$\mathbf{g}_\beta$	[1e-4 1e-4 1e-4]^T

tions). Note that it's the sole responsibility of the designer/operator to translate their objectives to an adequately developed FIS. Moreover, it should be remembered that the proposed scheme's performance is highly sensitive to the time step used for simulation. The smaller it will be, the more efficiently the FIS will track changes and produce corresponding actions. Conversely, the higher time step causes FIS to inadequately track the changes and produce poor control actions. In the current study, a fixed time step size of 0.00001s was used. Similarly, it should be noted that for current research, the variable "*r*" from equation (32) is made tuneable as given in Table 6. Equivalently, all the parameters of equation (32) can be made tuneable or the FIS with constant output MFs can also be used.

3.1.3. Voltage generation

The proposed controller's control forces cannot be directly delivered to the MRD since the controller creates the force signals, whereas the MRD requires a voltage or current signal. Therefore, a transformation step is needed to generate voltage. For that generation, either an inverse model of the MR damper is formulated, or a clipped algorithm can be used [61]. In this study, the inverse Bingham model of the MR damper is developed, as shown in eq. (42), using eq. (41) [56]. This inverse model will compute the appropriate voltage based on the proposed controller's control command.

$$f_{MR} = f_c \operatorname{sgn}(\dot{x}) + c_0 \dot{x} + f_0 \tag{41}$$

$$V = \frac{f_{MR} - c_0 \dot{x} + f_0}{f_c \operatorname{sgn}(\dot{x})} \tag{42}$$

Where, f_{MR} = command voltage provided by the proposed controller, c_o = damping coefficient; and f_c = frictional force, which is related to fluid yield stress and f_0 = offset value to adjust a nonzero force value due to the accumulator [56].

4. Results and discussion

4.1. Earthquake excitation

The building is subjected to the following 11-time scaled North-South (N–S) components of the historical earthquake accelerograms and their Fourier Amplitude Spectra (FAS) are shown in Fig. 16.

a) El Centro N–S component of 1940 Imperial valley earthquake; M_w = 6.4, PGA = 3.417 m/s^2
b) Hachinohe N–S component of Toka-Chi-Oki 1968 earthquake; M_w = 8.3, PGA = 2.250 m/s^2
c) Northridge 1994 earthquake at Sylmar station; N–S component M_w = 6.7, PGA = 8.2676 m/s^2
d) Kobe N–S component of Great Hanshin-Awaji 1995 earthquake; M_w = 6.9, PGA = 5.03 m/s^2
e) Chi-Chi N–S component of Chi-Chi earthquake 1999 earthquake; M_w = 7.6, PGA = 4.17 m/s^2
f) Erzincan N–S component of Erzincan earthquake 1992 earthquake; M_w = 6.7, PGA = 5.15 m/s^2
g) North Palm Spring 1992 earthquake N–S component; M_w = 6, PGA = 6.12 m/s^2
h) Bolu N–S component of Duzce earthquake 1999 earthquake; M_w = 6.9, PGA = 7.28 m/s^2
i) Northridge 1994 earthquake at Rinaldi station; N–S component M_w = 6.7, PGA = 4.72 m/s^2
j) Kocaeli earthquake 1999 earthquakes recorded at Gebze Tubitak Marmara Arastirma Merkezi; N–S component M_w = 7.4, PGA = 2.6170 m/s^2
k) Parkfield, California 2004 earthquakes; M_w = 6, PGA = 4.257 m/s^2

Where the Imperial Vellay (El Centro), Toka-Chi-Oki (Hachinohe), Great hanshin-Awaji (Kobe), Chi-Chi, Bolu (Duzce), Kocaeli (Gebze) belongs to the far field earthquakes their frequency contents can be seen in Fig. 16 (a, b, d, e, h and j). Where as, the Northridge (Sylmar), Erzincan, North Palm Spring, Northridge (Rinaldi) and Parkfield belongs to near field earthquakes their frequency contents can be seen in Fig. 16 (c, f, g, i and k).

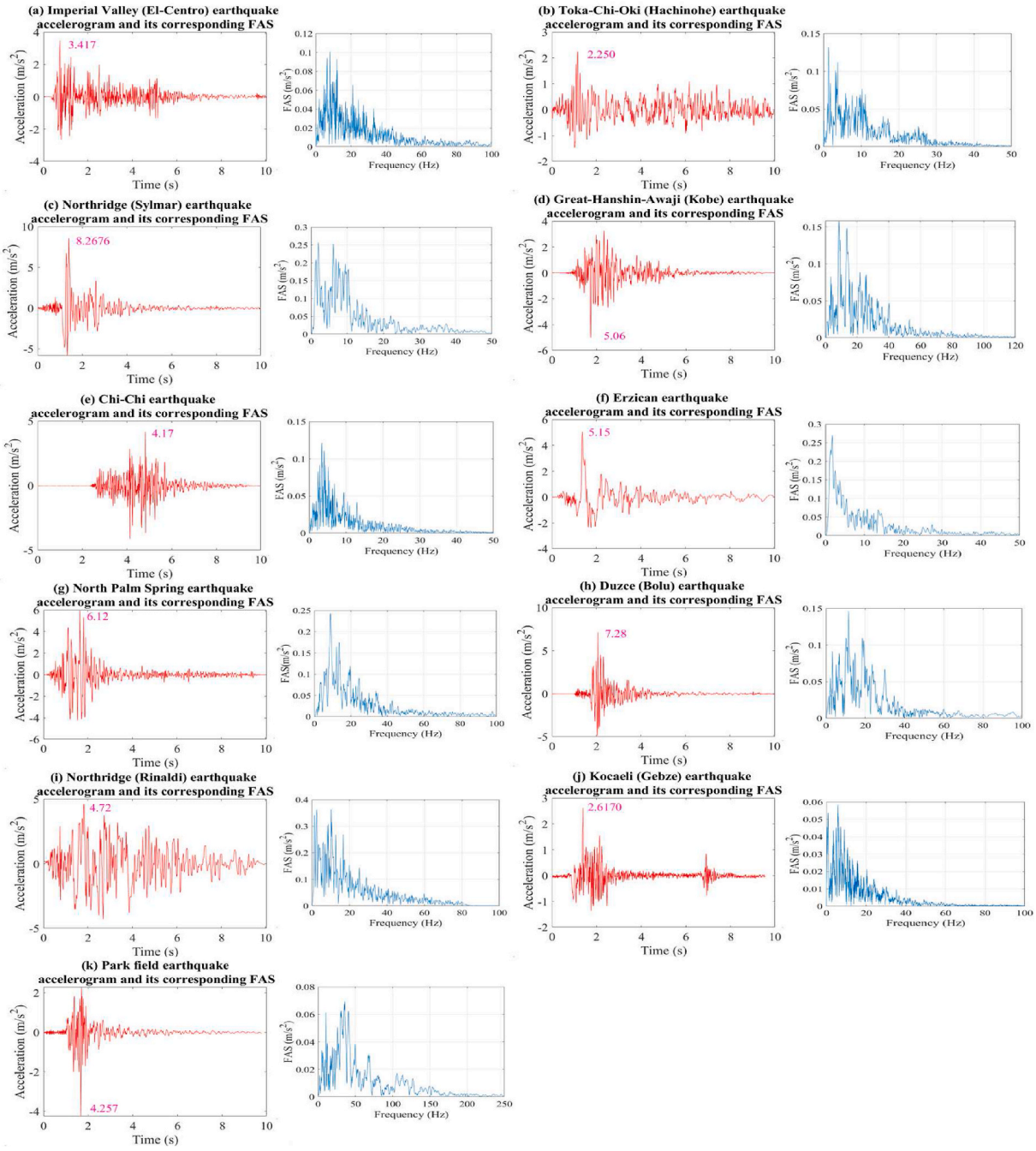

Fig. 16. Historic earthquake accelerograms and their Fourier Amplitude Spectra (FAS).

4.2. Comparison control methodologies

4.2.1. LQR

The LQR is an extensively exploited method in the control domain because of its ease of use and effectiveness. In this approach, an optimal feedback gain is determined so that there is a controlled force $\boldsymbol{f}_c(t) = -\boldsymbol{G}_{lqr}\boldsymbol{z}(t)$ attained through minimizing the following cost function j in the following equation [62,63].

$$j = \int_{t0}^{\infty} \left[\boldsymbol{z}(t)^T \boldsymbol{Q}_{lqr} \boldsymbol{z}(t) + \boldsymbol{f}_c(t)^T \boldsymbol{R}_{lqr} \boldsymbol{f}_c(t)\right] dt \tag{43}$$

Where, G_{lqr} is a gain matrix and, $Q_{lqr} and R_{lqr}$ are symmetric positive semidefinite and symmetric positive definite matrix. In the current research, the commonly used values of these matrices were chosen since they produce better results, as presented in the following equation [63,64].

$$Q_{lqr} = \frac{1}{2}\begin{bmatrix} K & 0 \\ 0 & M \end{bmatrix} and, \tag{44}$$

$$R_{lqr} = 1x10^{-5} I_{(n\times n)}$$

4.2.2. Fuzzy tuned PID (FT-PID)

The development of the proposed control methodology gives an online fuzzy-tuned PID (FT-PID) controller as a by-product as discussed in sub-section 3.1.2.1. of section 3.1.2. The FIS is developed to tune the parameters of a classic PID controller and further utilized for comparison. Furthermore, the purpose of doing so is to illustrate the effectiveness of the proposed controller.

4.3. Proposed controllers performance and structure responses

This section provides the graphical representation of the peak responses of the structure for the uncontrolled, LQR, FT-PID, and the proposed ST-BELBIC controller cases. The maximum displacement and absolute acceleration responses of third story of the building under Imperial Valley (EL-Centro), Kobe, and North Palm Springs earthquakes are presented in Fig. 17 (a and d), 17 (b and e), and 17 (c and f). Furthermore, unders these earthquakes the peak displacement and absolut acceleration response of the building at each floor level can be evidenced in Fig. 17(g–i) and 17 (j-l) which represents the higher performance of the proposed controller in reducing the maximum response of the building.

4.4. Performance indexes

To quantitatively and precisely access the comparative performance of the proposed controllers, a set of performance evaluation indexes are constructed in terms of peak and root mean square (RMS) and control performance as provided in eq. (45)–(52).

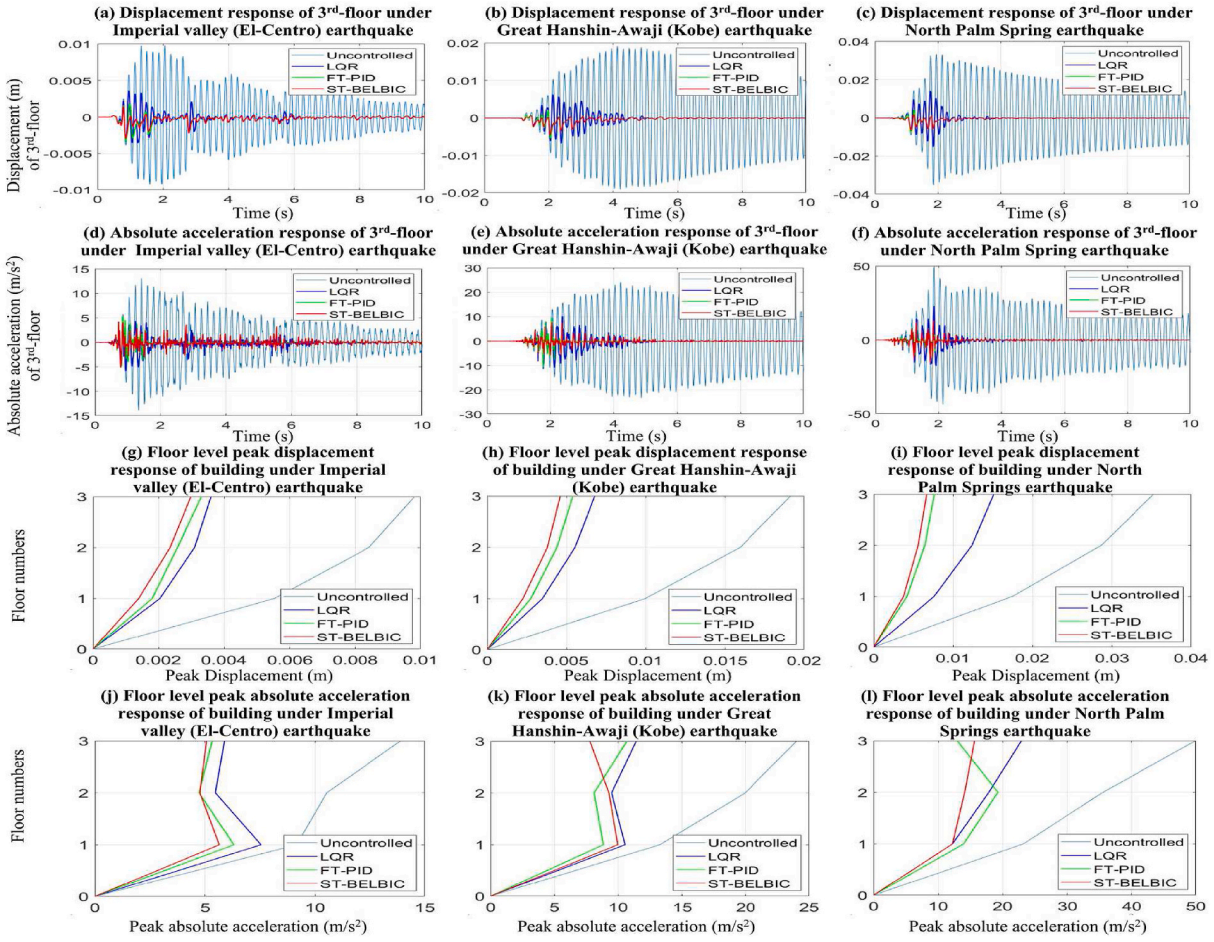

Fig. 17. Comparison of structural response records under El-Centro, Kobe and North Palm Springs eathquake

$$J1 = max\left\{\frac{\max|x_i(t)|}{x_{un}^{max}}\right\} \tag{45}$$

$$J2 = max\left\{\frac{\max|\dot{x}_i(t)|}{\dot{x}_{un}^{max}}\right\} \tag{46}$$

$$J3 = max\left\{\frac{\max|\ddot{x}_i(t)|}{\ddot{x}_{un}^{max}}\right\} \tag{47}$$

$$J4 = max\left\{\frac{\max|V_b(t)|}{V_{b,un}^{max}}\right\} \tag{48}$$

$$J5 = max\left\{\frac{\max|V_1(t)|}{V_{1,un}^{max}}\right\} \tag{49}$$

$$J6 = max\left\{\frac{\max x_i(t)}{\widehat{x_{un}^{max}}}\right\} \tag{50}$$

$$J7 = max\left\{\frac{\max \ddot{x}_i(t)}{\widehat{\ddot{x}_{un}^{max}}}\right\} \tag{51}$$

$$J8 = max\left\{\frac{\max|f_{c,i}(t)|}{W}\right\} \tag{52}$$

Where *J1*, *J2,* and *J3* in eq. (45)–(47) represent the peak displacement, velocity, and absolute acceleration response. The variables $x_i(t)$, $\dot{x}_i(t)$ *and,* $\ddot{x}_i(t)$ are the displacement, velocity and, absolute acceleration of the *i*th floor of controlled structure. The variables x_{un}^{max}, $\dot{x}_{un}^{max}$ and $\ddot{x}_{un}^{max}$ are maximum displacement, velocity and acceleration response of uncontrolled structure. Furthermore, two indexes based on the shear of the structure is formulated as given in eqs. (48) and (49), where *J4* presents the peak base shear and *J5* presents the peak superstructure (first story) shear. Where $V_b(t)$ presents the base shear of the controlled structures and $V_1(t)$ presents the shear at the first story level. Additionally, $V_{b,un}^{max}$ *and* $V_{1,un}^{max}$ represents the maximum base and superstructure shear of the uncontrolled structure. In the above-discussed criteria, the notion $|\cdot|$ stands for the corresponding vector's magnitude.

Correspondingly, the criteria presented in eqs. (50) and (51) specify the RMS normalized peak displacement and absolute acceleration responses of the structure. In these criteria's the notion $\|\cdot\|$ stands for the RMS of the corresponding vector's magnitude. Whereas, $\widehat{x_{un}^{max}}$ *and* $\widehat{\ddot{x}_{un}^{max}}$ represents the RMS of the displacement and absolute acceleration responses of the uncontrolled structure. Also, for scheming the peak control force generated by all the devices the *J8* criteria are used. Where the $f_{c,i}(t)$ presents the control force in the ith MRD and *W* corresponds the seismic weight of the superstructure. The values of these indexes, under 11 earthquakes, were determined to evaluate the proposed controllers' performance. A linear quadratic regulator (LQR), FT-PID, and ST-BELBIC system are simulated to establish a comparative analysis. The values of all these indexes for various controllers are shown in Table 8.

As presented in Table 8 the *J1* criteria show the peak displacement response that has been calculated under different earthquakes. For comparison of different controllers, the mean value of this criteria is calculated for each controller. The proposed ST-BELBIC controller has the finest value for this criterion with 0.4234, which is lower than the quantities determined for all the other controllers. Furthermore, the proposed ST-BELBIC mean value measured by the structure's peak displacement response in *J1* is lowered by 17.06% compared to LQR and 13.04% compared to the FT-PID controller.

Furthermore, the performance of FT-PID in reducing the displacement response also showed a 4.04% reduction when compared to the LQR controller. These results demonstrate that ST-BELBIC outperforms the competing controllers in terms of peak displacement reduction. Moreover, the proposed controller had a significant impact in lowering the structure's *J2* (peak velocity) responses. The reduction in *J2,* mean values for the ST-BELBIC is 33.29 and 10.06% compared to the LQR and FT-PID controllers. At the same time, the FT-PID performance comparative to LQR controller displays a 23.4269% reduction.

In terms of the calculated peak acceleration responses *J3*, the proposed ST-BELBIC controller manage to reduce the structure's acceleration response by 16.04% to the LQR and rectify the FT-PID controller's deficiencies by 24.72%. Furthermore, the base shear of the structure was also calculated, and the performance of the proposed ST-BELBIC can be evidenced in Table 8. The reduction of the peak base shear *J4* is 13.24 and 15.93% compared to LQR and FT-PID controllers. Moreover, ST-BELBIC performance for the *J5* index Peak superstructure shear shows a significant reduction of 14.53 and 15.9% compared to LQR and FT-PID controllers. The results demonstrate that the proposed controller fully improved the response of FT-PID controller concerning *J3*, *J4* and *J5* performance indexes.

To better quantify the results, the RMS of the peak displacement *J6* and acceleration *J7* responses were also presented. As can be found, for *J6* a 23.24 and 14.87% difference is remarked for LQR and FT-PID controllers. Whereas for the FT-PID this difference is given as 8.45%. Furthermore, For *J7* it's been calculated a total 32.19 and 3.59% reduction compared to LQR and FT-PID controllers.

Although the optimal generation of control force was not an objective of the current study, for providing a baseline for future study and demonstrating the potential of ST-BELBIC in improving the control performance, an index of control force *J8* is also pre-

Table 8
Performance indexes for comparison of LQR, FT-PID, and ST-BELBIC.

index	Controller	*El-Centro*	*Hachinohe*	*Sylmar*	*Kobe*	*Chi-Chi*	*Erzincan*	*North Palm Spring*	*Bolu*	*Rinaldi*	*Gebze*	*Parkfield*	*Average*
J1	LQR	0.3664	0.6190	0.6136	0.3538	0.3518	**0.9096**	0.4281	0.4897	0.4337	0.4968	0.4634	0.5024
	FT-PID	0.3365	0.7592	0.6986	0.2820	0.3873	0.9923	0.2164	0.3663	0.2147	0.5568	0.4972	0.4825
	ST-BELBIC	**0.3040**	**0.5574**	**0.6044**	**0.2404**	**0.3441**	0.9120	**0.1887**	**0.3660**	0.2147	**0.4934**	**0.4318**	**0.4234**
J2	LQR	0.4174	0.6172	0.6934	0.4135	0.4656	0.7657	0.4591	0.5589	0.3866	0.4174	0.5860	0.5255
	FT-PID	0.3795	0.7542	**0.5378**	0.2436	0.4408	0.8141	0.1895	0.2650	0.1893	0.3795	**0.3751**	0.4153
	ST-BELBIC	**0.3343**	**0.5031**	0.5889	**0.2098**	**0.3037**	**0.7331**	**0.1852**	**0.2648**	**0.1622**	**0.3343**	0.5109	**0.3755**
J3	LQR	0.5425	0.6597	0.8512	0.4750	**0.5120**	1.2137	0.4587	0.5375	0.3724	0.6959	0.9997	0.6653
	FT-PID	0.4538	0.7843	1.0089	0.4450	1.4265	1.0684	0.3857	0.4818	0.4624	0.7408	0.7319	0.7263
	ST-BELBIC	**0.4062**	**0.6592**	**0.8040**	**0.4151**	0.6513	**0.9105**	**0.3131**	**0.4815**	**0.2867**	**0.5732**	**0.7306**	**0.5665**
J4	LQR	0.5626	**0.6509**	0.8445	0.5489	**0.5945**	1.4532	0.4876	0.6426	0.3771	0.7331	1.0571	0.7229
	FT-PID	0.4873	0.7501	0.9584	0.4827	1.1643	1.2043	0.4250	0.5698	0.4394	0.7698	0.9185	0.7427
	ST-BELBIC	**0.4611**	0.6531	**0.8324**	**0.4720**	0.6299	**1.0556**	**0.3863**	**0.5696**	**0.3285**	**0.6616**	**0.9144**	**0.6331**
J5	LQR	0.4649	0.6638	0.8358	0.4750	**0.5547**	1.2707	0.4769	0.6237	0.3713	0.6120	1.0158	0.6695
	FT-PID	0.4117	0.6944	0.9604	0.4275	1.2690	1.0419	0.3770	0.5330	0.3379	0.6373	**0.7772**	0.6788
	ST-BELBIC	**0.4028**	**0.6174**	**0.8072**	**0.3878**	0.6262	**0.9326**	**0.3481**	**0.5329**	**0.2897**	**0.5854**	0.8365	**0.5788**
J6	LQR	0.2224	0.3380	0.2258	0.1437	0.1394	0.3816	0.1693	0.1486	0.2066	0.1704	0.4313	0.2343
	FT-PID	0.1654	0.3856	0.1725	0.0764	0.1531	0.4502	0.0740	0.1081	0.1252	0.1895	0.4680	0.2153
	ST-BELBIC	**0.1379**	**0.3216**	**0.1689**	**0.0723**	**0.1271**	**0.3633**	**0.0695**	**0.1079**	**0.1250**	**0.1572**	0.3901	**0.1855**
J7	LQR	0.2554	0.3813	0.2664	0.1743	0.2518	0.3873	0.1902	0.1931	0.2005	0.2529	0.5645	0.2834
	FT-PID	0.1823	0.3123	**0.1677**	**0.0876**	0.3062	**0.2088**	**0.0802**	0.1314	**0.0969**	0.2537	**0.5084**	0.2123
	ST-BELBIC	**0.1622**	**0.3014**	0.1914	0.1005	**0.2311**	0.2185	0.1061	**0.1311**	0.1100	**0.1905**	0.5100	**0.2048**
J8	LQR	**0.8364**	**0.9125**	1.1330	**1.3574**	**1.1254**	**0.8691**	**1.3026**	**1.1963**	**1.0774**	**0.9006**	**0.7092**	**1.0382**
	FT-PID	3.0499	2.7627	1.0387	3.4341	2.0592	1.6909	5.8827	3.3746	6.4062	2.6193	1.2020	3.0473
	ST-BELBIC	2.3493	2.3953	**1.0224**	3.2200	2.1561	1.6749	5.8105	3.3665	5.4058	2.3597	1.1350	2.8087

sented. The control force index for the proposed ST-BELBIC surprisingly shows an 8.14% reduction when compared to FT-PID. Moreover, for better understanding, the results are displayed in Fig. 18. Where, Fig. 18-(a-h) represents the visual representation of *J1-J8* indexes and their average values are presented in Fig. 18(i) respectively.

Lastly, the voltage variations generated by the FT-PID and ST-BELBIC controllers and their associated damping force delivered by the MR damper are shown in Fig. 19. When it comes to ST-BELBIC controlled structure under El-Centro and Kobe excitations, the voltage supplied to the MRD is presented in Fig. 19 (e) and (g), responding accordingly to the increase in applied excitation on the structure. Therefore, in the proposed controller, if the applied excitation increases, the voltage provided to the control device increases until the signal limit is reached. The signal command generates a range of voltages between 0 and 2.25 V. In these plots, it can be confirmed that the controller can fully maintain a constant voltage supply.

Furthermore, the corresponding damping force produced by ST-BELBIC controlled MRD is presented in Fig. 19 (a & c). The plot clearly illustrated that the proposed controller's command voltage and corresponding force agreed that maximal voltage supply is constantly available whenever the excitation increases and reaches a peak. As a result, the system will operate intelligently by generating necessary damping forces to ovoid instability in the system and ensuring proper energy dissipation.

Moreover, it is demonstrated in Fig. 19. (f & h) even when the change in acceleration is high, the controller based on FT-PID shows behaviour that closely mirrors the slightly changing voltage provided to the structure. As a result, the voltage range somehow doesn't remain consistent during periods of change in ground acceleration. That finally results in a poor amount of energy dissipation in the system. Additionally, it is also evidence from Fig. 19 that the proposed controller fully tracks the response by maintaining a good balance between applied force and excitations. One can deduce that the proposed controller can control the seismic response of structure compared to the other controllers and help adjust the mistuned response of the other smart controller like FT-PID controller by simultaneously utilizing its reasoning and learning capabilities.

5. Conclusions

This study developed a new self-tuned brain emotional learning-based intelligent controller (ST-BELBIC) algorithm to attenuate the response of three-story scaled building structure subjected ground excitations. The design of the proposed controller was based on two main objectives (i) develop a self-tuned BELBIC and; (ii) improve the response of the cascaded controller. These objectives were achieved by integrating a fuzzy supervisor/tuner to empower the proposed controller to modify its parameters/gains adaptively, such as the system's performance matches the required response for changing operating circumstances.

To compare the performance of the proposed controller, an LQR and the FT-PID controllers were also developed. The results show that an ST-BELBIC controller achieves more outstanding performance in attenuating the responses of the structure when compared to an LQR and FT- PID controller using a set of performance indexes. Based on the results of the study, the proposed controller showed a 17.06 and 13.04% reduction in *J1* (peak displacement), 33.29 and 10.06% reduction in *J2* (peak velocity), and 16.06 and 24.72% reduction in *J3* (peak acceleration) compared to LQR and FT-PID controllers respectively. Moreover, for the peak Base shear (*j4*) and super structure shear (*j5*) indexes the proposed controller showed extraordinary performance. For *j4* it showed 13.24 and 15.93% and for *j5* it showed 14.53 and 15.9% reduction compared to LQR and FT-PID. Where as the RMS indexes of peak displacement *j6* it had

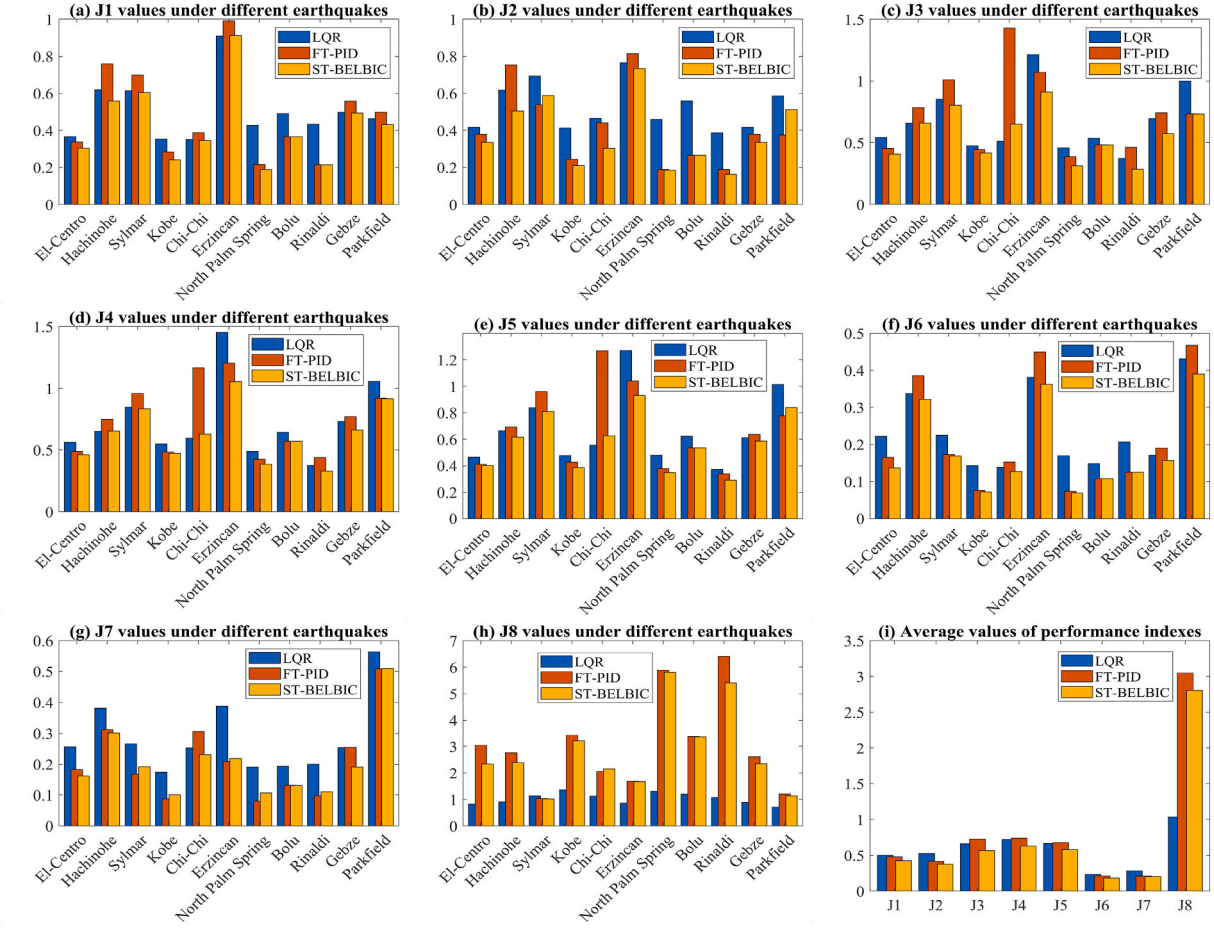

Fig. 18. Comparison of performance criteria J1-J8 of LQR, FT-PID, ST-BELBIC.

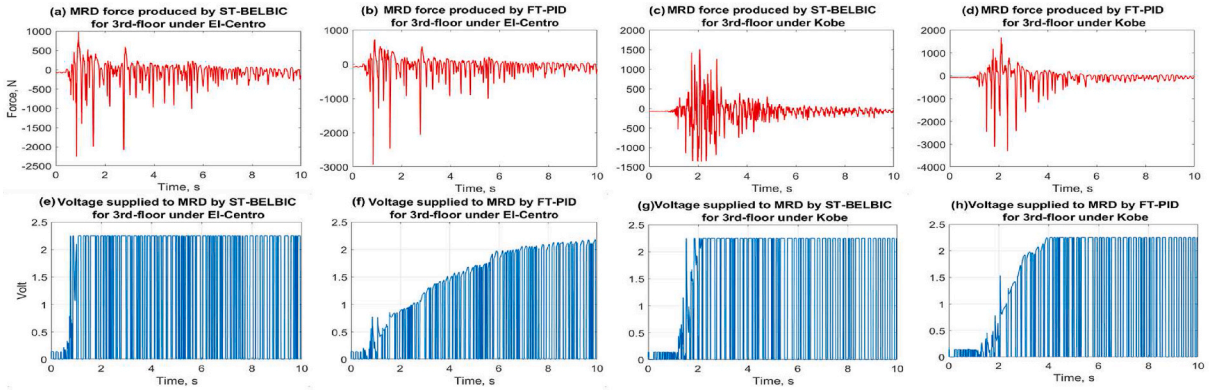

Fig. 19. Supplied voltage and damping force produced by MRD.

shown 23.24 and 14.87% reduction and for RMS of peak absolute accelearation *j7* its had shown 32.19 and 3.59% reduction compared to LQR and BELBIC. Although the proposed control was not developed for optimal generation of control force it improved the force generation of FT-PID by 8.1%. In general the proposed controller can reduce the structural response and neutralize the inadequacies of the cascaded controller like in our study; it was an FT-PID.

The novelty of ST-BELBIC is a control strategy that is self-tuneable and a data-driven control rather than conventional model-based controllers (MBC). Furthermore, this study also demonstrates the performance of the model-free controllers when two intelligent systems (fuzzy and BEL) are combined to handle and improve the deficiencies presented in each other. The proposed controller is also a perfect example of modular design for adaptive control where the conventional MBC PID was tuned online by FIS to generate

BELBICs signals. Conclusively all these systems help formulate the best responsive control algorithm. It should be noted that the proposed ST-BELBIC is not limited to semiactive control cases. Still, it can be investigated on active control cases of smart civil and mechanical structures.

Future studies will consider the potentials of FIS tuned BELBIC for achieving multi objectives (response attenuation and optimal control force generation) in the vibration control of smart civil structures. Moreover, it is recommended to trial BEL with different formulations of intelligent/conventional systems to increase the adaptivity and robustness of the next generation of smart civil structures.

CRediT author statement

Muhammad Usman Saeed: Designed the Theoretical Model, Performed the Computational Framework, and Wrote the Manuscript. Zuoyu Sun: Supervision at Main University, Supervised the work, provided Critical Feedback, Analyzed and Verified the Analytical Methods, correction of the Prepared manuscript by First Author. Said Elias: at University of Twente also Supervised the work, Enrichment of the Proposed Model and Computation, interpreting and Validating Results, Finalizing-Original draft, Reviewing and Editing.

Declaration of competing interest

The authors declare that they have no known competing financial interests or personal relationships that could have appeared to influence the work reported in this paper.

References

[1] A. Yanik, U. Aldemir, A simple structural control model for earthquake excited structures, Engineering Structures 182 (2019) 79–88.
[2] N. Talyan, S. Elias, V. Matsagar, Earthquake response control of isolated bridges using supplementary passive dampers, Practice Periodical on Structural Design and Construction 26 (2) (2021) 04021002.
[3] S. Panchanan, S. Banerjee, R.S. Jangid, P. Kumar, Soil–structure interaction effect on seismic response of controlled asymmetric buildings, Proceedings of the Institution of Civil Engineers-Structures and Buildings (2021) 1–14.
[4] L. Suresh, K.M. Mini, Effect of multiple tuned mass dampers for vibration control in high-rise buildings, Practice Periodical on Structural Design and Construction 24 (4) (2019) 04019031.
[5] S. Elias, V. Matsagar, Research developments in vibration control of structures using passive tuned mass dampers, Annual Reviews in Control 44 (2017) 129–156.
[6] M. Zucca, N. Longarini, M. Simoncelli, A.M. Aly, Tuned mass damper design for slender masonry structures: a framework for linear and nonlinear analysis, Applied Sciences 11 (8) (2021) 3425.
[7] S.J. Suthar, R.S. Jangid, Multiple tuned liquid sloshing dampers for across-wind response control of benchmark tall building, Innovative Infrastructure Solutions 7 (1) (2022) 1–15.
[8] R.S. Jangid, Optimum tuned inerter damper for base-isolated structures, Journal of Vibration Engineering & Technologies (2021) 1–15.
[9] V.R. Panchal, R.S. Jangid, B.B. Shobhana, Seismic performance of bridges with variable friction pendulum system, International Journal of Structural Engineering 11 (4) (2021) 342–363.
[10] M. Bozorgvar, S.M. Zahrai, Semi-active seismic control of buildings using MR damper and adaptive neural-fuzzy intelligent controller optimized with genetic algorithm, Journal of Vibration and Control 25 (2) (2019) 273–285.
[11] H.S. Kim, J.W. Kang, Semi-active fuzzy control of a wind-excited tall building using multi-objective genetic algorithm, Engineering Structures 41 (2012) 242–257.
[12] A.M. Aly, H. Gol-Zaroudi, M. Rezaee, A framework for vibration attenuation in traffic mast arm structures under wind loads, Experimental Techniques (2021) 1–19.
[13] Q. Wang, J. Wang, X. Huang, L. Zhang, Semiactive Nonsmooth Control for Building Structure with Deep Learning, Complexity, 2017, 2017.
[14] A.Y. Rababah, K.A. Bani-Hani, W.S. Baraham, Adaptive neural network controller for nonlinear highway bridge benchmark, Jordan Journal of Civil Engineering 13 (2) (2019).
[15] R.W. Soares, L.R. Barroso, O.A. Al-Fahdawi, Response attenuation of cable-stayed bridge subjected to central US earthquakes using neuro-fuzzy and simple adaptive control, Engineering Structures 203 (2020) 109874.
[16] M.U. Saeed, Z. Sun, S. Elias, Research developments in adaptive intelligent vibration control of smart civil structures, Journal of Low Frequency Noise, Vibration and Active Control 0 (0) (2021) 1–38.
[17] B. Blachowski, N. Pnevmatikos, Neural network based vibration control of seismically excited civil structures, Periodica Polytechnica Civil Engineering 62 (3) (2018) 620–628.
[18] L. Lara, J. Brito, C.A.G. Gallego, Structural control strategies based on magnetorheological dampers managed using artificial neural networks and fuzzy logic, Revista UIS Ingenierías 16 (2) (2017) 227–242.
[19] N. Rathi, H.P. Singh, S. Kumar, Modeling of a neural network based controller for vibration suppression of a building structure, in: AIP Conference Proceedings, vol. 1975, AIP Publishing LLC, 2018, p. 30018, 1.
[20] M. Zabihi-Samani, M. Ghanooni-Bagha, Optimal semi-active structural control with a wavelet-based cuckoo-search fuzzy logic controller, Iranian Journal of Science and Technology, Transactions of Civil Engineering 43 (4) (2019) 619–634.
[21] A. Bathaei, S.M. Zahrai, M. Ramezani, Semi-active seismic control of an 11-DOF building model with TMD+ MR damper using type-1 and-2 fuzzy algorithms, Journal of Vibration and Control 24 (13) (2018) 2938–2953.
[22] K. Faraji, Seismic Performance of a Semi-active MR Damper Improved by Fuzzy Control System, Doctoral dissertation, Concordia University, 2018.
[23] M. Fatourechi, C. Lucas, A.K. Sedigh, Reducing control effort by means of emotional learning, in: Proceedings of 19th Iranian Conference on Electrical Engineering, vol. 41, 2001, pp. 1–41.
[24] C. Balkenius, J. Morén, A computational model of context processing, in: 6th International Conference on the Simulation of Adaptive Behaviour, 2000.
[25] C.B.J. MorÉn, Emotional learning: a computational model of the amygdala, Cybernetics & Systems 32 (6) (2001) 611–636.
[26] J. Moren, Emotion and Learning: a Computational Model of the Amygdala [Ph. D. Thesis], Lund University, Lund, Sweden, 2002.
[27] C. Lucas, D. Shahmirzadi, N. Sheikholeslami, Introducing BELBIC: brain emotional learning based intelligent controller, Intelligent Automation & Soft Computing 10 (1) (2004) 11–21.
[28] M.H. Soreshjani, G.A. Markadeh, E. Daryabeigi, N.R. Abjadi, A. Kargar, Application of brain emotional learning-based intelligent controller to power flow control with thyristor-controlled series capacitance, IET Generation, Transmission & Distribution 9 (14) (2015) 1964–1976.
[29] S. Khorashadizadeh, M.M.J.R. Fateh, Uncertainty estimation in robust tracking control of robot manipulators using the Fourier series expansion 35 (2) (2017) 310.
[30] S. Khorashadizadeh, M. Mahdian, January). Voltage tracking control of DC-DC boost converter using brain emotional learning, in: 2016 4th International Conference on Control, Instrumentation, and Automation (ICCIA), IEEE, 2016, pp. 268–272.

[31] S. Tong, Y. Li, Direct adaptive fuzzy backstepping control for a class of nonlinear systems, International Journal of Innovative Computing, Information and Control 3 (4) (2007) 887–896.
[32] E. Daryabeigi, H.A. Zarchi, G.A. Markadeh, J. Soltani, F. Blaabjerg, Online MTPA control approach for synchronous reluctance motor drives based on emotional controller, IEEE Transactions on Power Electronics 30 (4) (2014) 2157–2166.
[33] M.B. César, J. Gonçalves, J. Coelho, R.C. de Barros, Brain emotional learning based control of a SDOF structural system with a MR damper, in: CONTROLO 2016, Springer, Cham, 2017, pp. 547–557.
[34] S. Valizadeh, M.R. Jamali, C. Lucas, October). A particle-swarm-based approach for optimum design of BELBIC controller in AVR system, in: 2008 International Conference on Control, Automation and Systems, IEEE, 2008, pp. 2679–2684.
[35] M.B. César, J.P. Coelho, J. Gonçalves, June). Semi-active vibration control of a non-collocated civil structure using evolutionary-based BELBIC, in: Actuators, vol. 8, Multidisciplinary Digital Publishing Institute, 2019, p. 43, No. 2.
[36] M.B. César, J. Paulo Coelho, J. Gonçalves, June). Evolutionary-based BEL controller applied to a magneto-rheological structural system, in: Actuators, vol. 7, Multidisciplinary Digital Publishing Institute, 2018, p. 29, No. 2.
[37] M.H. Valipour, K.N. Maleki, S.S. Ghidary, Optimization of emotional learning approach to control systems with unstable equilibrium, in: Software Engineering, Artificial Intelligence, Networking and Parallel/Distributed Computing, Springer, Cham, 2015, pp. 45–56.
[38] M.H. El-Saify, A.M. El-Garhy, G.A. El-Sheikh, Brain emotional learning based intelligent decoupler for nonlinear multi-input multi-output distillation columns, Mathematical Problems in Engineering 2 (2017) 1–13.
[39] D.H. Zelleke, V.A. Matsagar, Energy-based predictive algorithm for semi-active tuned mass dampers, The Structural Design of Tall and Special Buildings 28 (12) (2019) e1626.
[40] M. Jafari, A.M. Shahri, S.H. Elyas, Optimal tuning of brain emotional learning based intelligent controller using clonal selection algorithm, in: ICCKE 2013, IEEE, 2013, pp. 30–34.
[41] S. Jafarzadeh, M.J. Motlagh, M. Barkhordari, R. Mirheidari, June). A new lyapunov based algorithm for tuning belbic controllers for a group of linear systems, in: 2008 16th Mediterranean Conference on Control and Automation, IEEE, 2008, pp. 593–595.
[42] N. Garmsiri, F. Najafi, Fuzzy tuning of brain emotional learning based intelligent controllers, in: 2010 8th World Congress on Intelligent Control and Automation, IEEE, 2010, pp. 5296–5301.
[43] S.A. Nahian, D.Q. Truong, K.K. Ahn, A self-tuning brain emotional learning–based intelligent controller for trajectory tracking of electrohydraulic actuator, Proceedings of the Institution of Mechanical Engineers, Part I: Journal of Systems and Control Engineering 228 (7) (2014) 461–475.
[44] H. Rouhani, M. Jalili, B.N. Araabi, W. Eppler, C. Lucas, Brain emotional learning based intelligent controller applied to neurofuzzy model of micro-heat exchanger, Expert Systems with Applications 32 (3) (2007) 911–918.
[45] T.L. Le, C.M. Lin, T.T. Huynh, Self-evolving type-2 fuzzy brain emotional learning control design for chaotic systems using PSO, Applied Soft Computing 73 (2018) 418–433.
[46] T.J. Ross, Fuzzy Logic with Engineering Applications, John Wiley & Sons, 2005.
[47] M. Mirrashid, H. Naderpour, Computational intelligence-based models for estimating the fundamental period of infilled reinforced concrete frames, Journal of Building Engineering (2021) 103456.
[48] Z.S. Huang, C. Wu, D.S. Hsu, Semi-active fuzzy control of mr damper on structures by genetic algorithm, Journal of Mechanics 25 (1) (2009) N1–N6.
[49] J.X. Xu, C.C. Hang, C. Liu, Parallel structure and tuning of a fuzzy PID controller, Automatica 36 (5) (2000) 673–684.
[50] S.J. Dyke, B.F. Spencer Jr., M.K. Sain, J.D. Carlson, Modeling and control of magnetorheological dampers for seismic response reduction, Smart materials and structures 5 (5) (1996) 565.
[51] B.F. Spencer Jr., S. Nagarajaiah, State of the art of structural control, Journal of structural engineering 129 (7) (2003) 845–856.
[52] A. Yanik, Seismic control performance indices for magneto-rheological dampers considering simple soil-structure interaction, Soil Dynamics and Earthquake Engineering 129 (2020) 105964.
[53] S. Panchanan, P. Kumar, S. Basu, R.S. Jangid, Seismic response of asymmetric structure with soil structure interaction using semi-active MR damper, in: Recent Advances in Computational Mechanics and Simulations, Springer, Singapore, 2021, pp. 457–468.
[54] D. Cruze, G. Hemalatha, S.V.S. Jebadurai, L. Sarala, D. Tensing, S.J.E. Christy, A review on the magnetorheological fluid, damper and its applications for seismic mitigation, Civil Engineering Journal 4 (12) (2018) 3058–3074.
[55] M. Ismail, F. Ikhouane, J. Rodellar, The hysteresis Bouc-Wen model, a survey, Archives of Computational Methods in Engineering 16 (2) (2009) 161–188.
[56] B. Spencer Jr., S.J. Dyke, M.K. Sain, J. Carlson, Phenomenological model for magnetorheological dampers, Journal of Engineering Mechanics 123 (3) (1997) 230–238.
[57] J.P. Coelho, T.M. Pinho, J. Boaventura-Cunha, J.B. de Oliveira, A new brain emotional learning Simulink® toolbox for control systems design, IFAC-PapersOnLine 50 (1) (2017) 16009–16014.
[58] A.R. Mehrabian, C. Lucas, J. Roshanian, Aerospace launch vehicle control: an intelligent adaptive approach, Aerospace Science and technology 10 (2) (2006) 149–155.
[59] T. Peng, Q. Zhu, M.O. Tokhi, Y. Yao, Fuzzy logic feedforward active noise control with distance ratio and acoustic feedback using Takagi–Sugeon–Kang inference, Journal of Low Frequency Noise, Vibration and Active Control 39 (1) (2020) 174–189.
[60] M.S. Hadi, I.Z.M. Darus, M.O. Tokhi, M.F. Jamid, Active vibration control of a horizontal flexible plate structure using intelligent proportional–integral–derivative controller tuned by fuzzy logic and artificial bee colony algorithm, Journal of Low Frequency Noise, Vibration and Active Control 39 (4) (2020) 1159–1171.
[61] Y. Kim, R. Langari, S. Hurlebaus, Semiactive nonlinear control of a building with a magnetorheological damper system, Mechanical systems and signal processing 23 (2) (2009) 300–315.
[62] A. Yanik, Absolute instantaneous optimal control performance index for active vibration control of structures under seismic excitation, Shock and Vibration 4 (2019) 1–13.
[63] O.A. Al-Fahdawi, L.R. Barroso, R.W. Soares, Simple adaptive control method for mitigating the seismic responses of coupled adjacent buildings considering parameter variations, Engineering Structures 186 (2019) 369–381.
[64] O.A. Al-Fahdawi, L.R. Barroso, Adaptive neuro-fuzzy and simple adaptive control methods for full three-dimensional coupled buildings subjected to bi-directional seismic excitations, Engineering Structures 232 (2021) 111798.